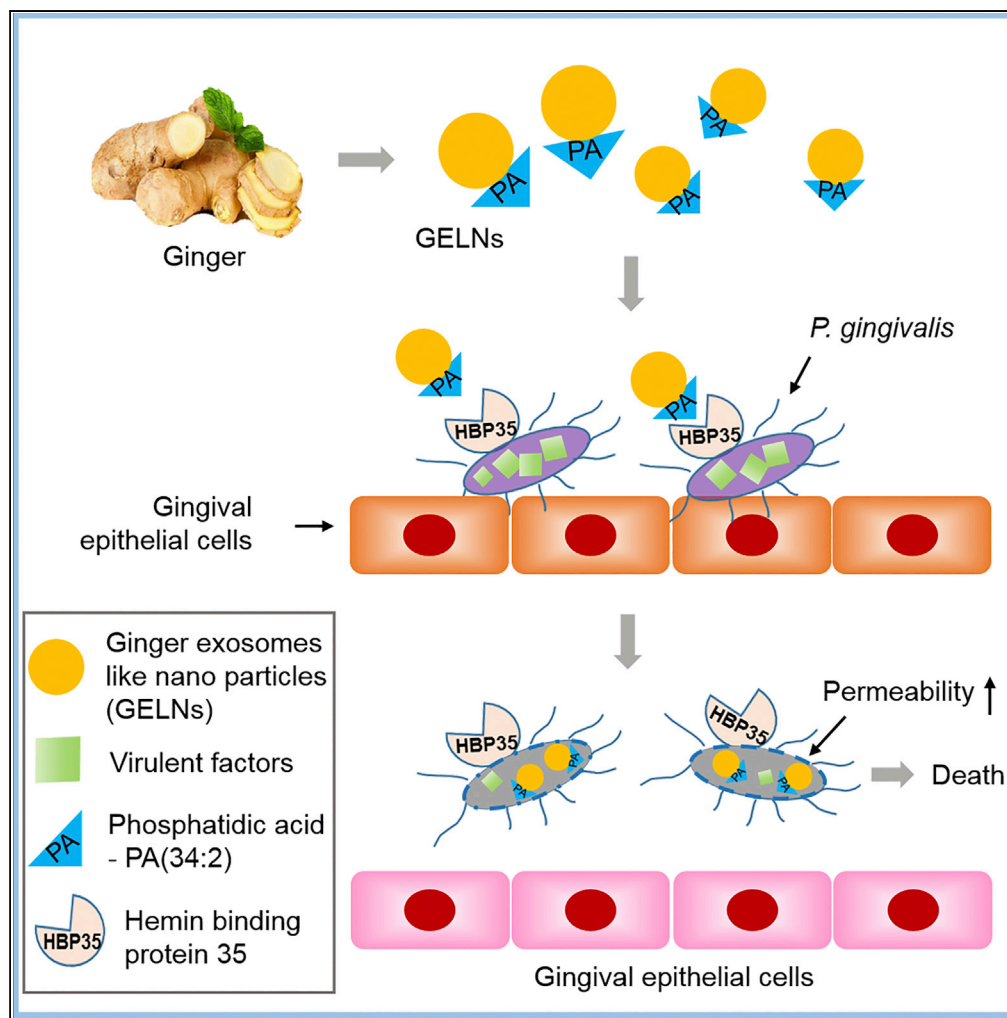**Article**

# Plant-Derived Exosomal Nanoparticles Inhibit Pathogenicity of *Porphyromonas gingivalis*



Kumaran Sundaram, Daniel P. Miller, Anil Kumar, ..., Juw W. Park, Richard J. Lamont, Huang-Ge Zhang

h0zhan17@louisville.edu

**HIGHLIGHTS**

Plant exosomes-like nanoparticles (ELNs) are selectively taken up by *P. gingivalis*

The degree of unsaturation of ELNs phosphatidic acid determines uptake specificity

ELN PA and miRs target multiple pathogenic factors of *P. gingivalis*

Orally taking ginger ELNs ameliorates bone loss induced by *P. gingivalis*

## Article

# Plant-Derived Exosomal Nanoparticles Inhibit Pathogenicity of *Porphyromonas gingivalis*

Kumaran Sundaram,[2] Daniel P. Miller,[5] Anil Kumar,[2] Yun Teng,[2] Mohammed Sayed,[3] Jingyao Mu,[2] Chao Lei,[2] Mukesh K. Sriwastva,[2] Lifeng Zhang,[2] Yan Jun,[2] Michael L. Merchant,[4] Liqing He,[8] Yuan Fang,[8] Shuangqin Zhang,[7] Xiang Zhang,[8] Juw W. Park,[3,6] Richard J. Lamont,[5] and Huang-Ge Zhang[1,2,9,*]

## SUMMARY

**Plant exosomes protect plants against infection; however, whether edible plant exosomes can protect mammalian hosts against infection is not known. In this study, we show that ginger exosome-like nanoparticles (GELNs) are selectively taken up by the periodontal pathogen *Porphyromonas gingivalis* in a GELN phosphatidic acid (PA) dependent manner via interactions with hemin-binding protein 35 (HBP35) on the surface of *P. gingivalis*. Compared with PA (34:2), PA (34:1) did not interact with HBP35, indicating that the degree of unsaturation of PA plays a critical role in GELN-mediated interaction with HBP35. On binding to HBP35, pathogenic mechanisms of *P. gingivalis* were significantly reduced following interaction with GELN cargo molecules, including PA and miRs. These cargo molecules interacted with multiple pathogenic factors in the recipient bacteria simultaneously. Using edible plant exosome-like nanoparticles as a potential therapeutic agent to prevent/treat chronic periodontitis was further demonstrated in a mouse model.**

## INTRODUCTION

Chronic infectious disease commonly involves large numbers of virulence factors that target several host factors in multiple pathways (Pan et al., 2014). Developing an effective therapeutic strategy that can inhibit a plurality of virulence factors without causing side effects requires a change from the current focus of delivering individual therapeutic agents to delivery of a package of therapeutic agents that can target multiple virulence factors simultaneously (Baron, 2013; Kauppi et al., 2003). No such ideal delivering vehicle that can selectively target pathogenic organisms and carry multiple therapeutic agents without causing toxicity is available. Recently, edible plant-derived exosome-like nanoparticles (ELNs) have been identified, and these consist of a large numbers of lipids, RNA including microRNAs (miRNAs), and proteins (Mu et al., 2014; Wang et al., 2013). It is well documented that edible plants are beneficial for human health and can prevent/treat chronic infectious diseases (Alvarez-Erviti et al., 2011; Zhuang et al., 2011). However, the cellular and molecular mechanism underlying the therapeutic effect on infectious disease by plants is not known. Since ELNs carry a large number and variety of molecules naturally (Mu et al., 2014; Xiao et al., 2018), we hypothesize that, upon ELNs being taken up by infectious agents, the ELN molecules can target multiple virulence factors simultaneously to prevent disease development.

*Porphyromonas gingivalis*, a Gram-negative anaerobe, is a major pathogen in chronic periodontitis, an inflammatory disease associated with dysbiotic host responses (Olsen et al., 2017). Periodontitis and periodontal pathogens have also been associated with serious systemic conditions including cardiovascular disease, type 2 diabetes mellitus, and adverse pregnancy outcomes (Liu et al., 2018; Reyes et al., 2018). *P. gingivalis* produces a number of virulence factors that enable colonization of oral surfaces, degradation of periodontal tissues, induction of destructive immune responses, and growth in the peptide- and hemin-rich inflammatory microenvironment. These include the FimA- and Mfa1-component fimbrial adhesins, arginine (Rgp)- and lysine (Kgp)-specific gingipain proteases, lipopolysaccharides, and hemin transport systems (Zenobia and Hajishengallis, 2015) (Lamont et al., 2018) (Bao et al., 2014).

Oral delivery of ginger exosome-like nanoparticles (GELNs) in mice leads to protection against alcohol-induced liver damage (Zhuang et al., 2015). Moreover, GELNs alter the gut microbiome composition and host physiology (Teng et al., 2018) leading us to test whether GELNs could be applied to treat/prevent

[1]Robley Rex Veterans Affairs Medical Center, Louisville, KY 40206, USA

[2]James Graham Brown Cancer Center, Department of Microbiology & Immunology, University of Louisville, CTRB 309, 505 South Hancock Street, Louisville, KY 40202, USA

[3]Department of Computer Engineering and Computer Science, University of Louisville, Louisville, KY 40202, USA

[4]Kidney Disease Program and Clinical Proteomics Center, University of Louisville, Louisville, KY, USA

[5]Department of Oral Immunology and Infectious Diseases, University of Louisville School of Dentistry, Louisville, KY 40202, USA

[6]KBRIN Bioinformatics Core, University of Louisville, Louisville, KY 40202, USA

[7]Department of Medicine, University of Chicago, Chicago, IL 60637, USA

[8]Department of Pharmacology and Toxicology, University of Louisville, Louisville, KY 40202, USA

[9]Lead Contact

*Correspondence: h0zhan17@louisville.edu

https://doi.org/10.1016/j.isci.2019.10.032

oral infectious disease. In this study, ginger-derived ELNs (GELNs) were tested for antagonism of *Porphyromonas gingivalis* virulence factors and for inhibition of pathogenicity in a chronic periodontitis mouse model. Our data suggest that GELNs are selectively taken up by *P. gingivalis* whereupon pathogenicity of the organism is reduced. Pathogenic processes impacted by GELNs include growth, attachment, entry, and proliferation in host cells, with consequent reduced virulence in a mouse model of periodontal disease.

## RESULTS

### Ginger Exosome-like Nanoparticles Are Selectively Taken up by *P. gingivalis* Leading to Inhibition of *P. gingivalis* Growth

Our previous reports have shown that GELNs have anti-inflammatory effects (Mu et al., 2014) via interaction with host hepatocytes (Zhuang et al., 2015), and moreover GELN miRNAs selectively promote beneficial bacterial growth in the intestine (Teng et al., 2018). Whether GELNs have a direct effect on pathogenic oral bacteria such as *P. gingivalis* is not known. To test this, *P. gingivalis,* along with the oral commensal *Streptococcus gordonii,* was incubated with different concentrations (0–6.0 × 10⁸ particles/mL) of PKH26-labeled GELNs for 1 h. fluorescence-activated cell sorting (FACS) analysis indicated that the GELNs were selectively taken up by *P. gingivalis* in a dose-dependent manner, whereas uptake of GELNs by *S. gordonii* was negligible (Figure 1A). *P. gingivalis* uptake of GELNs was further confirmed by confocal microscopy with fluorescently labeled *P. gingivalis* and GELNs (Figure 1B).

Uptake of GELNs led to inhibition of the growth of *P. gingivalis* in a dose- and time-dependent manner (Figures 1C and 1D). At a higher dose (6×10⁸ particles/mL), no growth of *P. gingivalis* was observed. Electron microscopy images further suggested that GELN treatment at the higher dose completely disrupted the morphology of *P. gingivalis* but not of *S. gordonii* (Figure 1D). Additionally, GELNs neither were taken up by *S. gordonii* nor inhibited the growth of this commensal. However, GELNs did inhibit the *in vitro* growth of other bacteria including *F. nucleatum, P. intermedia*, and *A. actinomycetemcomitans* (Figures S1C–S1E), which are associated with periodontitis.

Membrane depolarization has a profound impact on bacterial viability and signal transduction (Goldberg et al., 2013). Thus, we measured GELN effect on cytoplasmic membrane depolarization of *P. gingivalis* and *S. gordonii* using the membrane potential-sensitive dye diSC3-5 (Nusslein et al., 2006). The results showed that GELNs increased the depolarization of *P. gingivalis*. In contrast, GELNs did not affect the cytoplasmic membrane depolarization of *S. gordonii* (Figures S2A and S2B). In addition, we measured the *P. gingivalis* outer membrane barrier function by an ethidium bromide (EtBr) influx assay (Miki and Hardt, 2013). Our results showed that GELNs significantly increased fluorescence intensity in a dose-dependent manner (Figure S2C). Furthermore, we collected the supernatant from GELN-treated *P. gingivalis* and *S. gordonii* along with untreated control and analyzed these by SDS-PAGE electrophoresis. A large amount of proteins was released into the external milieu by GELN-treated *P. gingivalis* but not by GELN-treated *S. gordonii* (Figure S2D), indicating that interaction of GELNs with the *P. gingivalis* membrane leads to external release of cytoplasmic proteins. We also quantified metabolic products released from GELN-treated *P. gingivalis* (Figure S3), and the predicted role of these metabolic products is listed in Table S1. Collectively, the data indicate that GELNs are selectively taken up by pathogenic *P. gingivalis,* but not by commensal *S. gordonii,* leading to membrane perturbations and inhibition of *P. gingivalis* growth.

Edible plant exosomes, including GELNs, consist of a number of proteins, lipids, and RNAs including miRNA (Mu et al., 2014). Next, we determined which GELN-derived factor(s) specifically inhibits *P. gingivalis* growth. *P. gingivalis* was treated with different concentrations of total lipids derived from GELNs (lipidG) (0–5.0 × 10⁸ particles/mL) for 24 h and growth measured. LipidG significantly decreased *P. gingivalis* growth in a dose-dependent manner (Figure 2A). RNA sequencing analysis of GELN RNAs showed that miRNAs are enriched (Figure S4). Target sequencing analysis showed that these GELN miRNAs have potential target sequences in a variety of genes in *P. gingivalis* (Table S2). Based on the target genes in *P. gingivalis*, we selected miRNAs aly-miR159a-3p, gma-miR166u, and gma-miR166p to further determine whether miRNAs play a role in inhibition of *P. gingivalis* growth. *P. gingivalis* was transduced with GELN-derived miRNAs, and *P. gingivalis* growth was measured. As shown in Figure S5, these miRNAs did not affect the growth of *P. gingivalis,* supporting the notion that GELN lipids play a critical role in inhibition of *P. gingivalis* growth. Thus, we next determined whether GELN-derived total lipids (lipidG) and miRNA have synergetic effects on the growth of *P. gingivalis*. However, as shown in Figure S6, lipidG and miRNA from GLENs do not have a synergetic effect. Next, we investigated which GELN lipid(s) inhibits
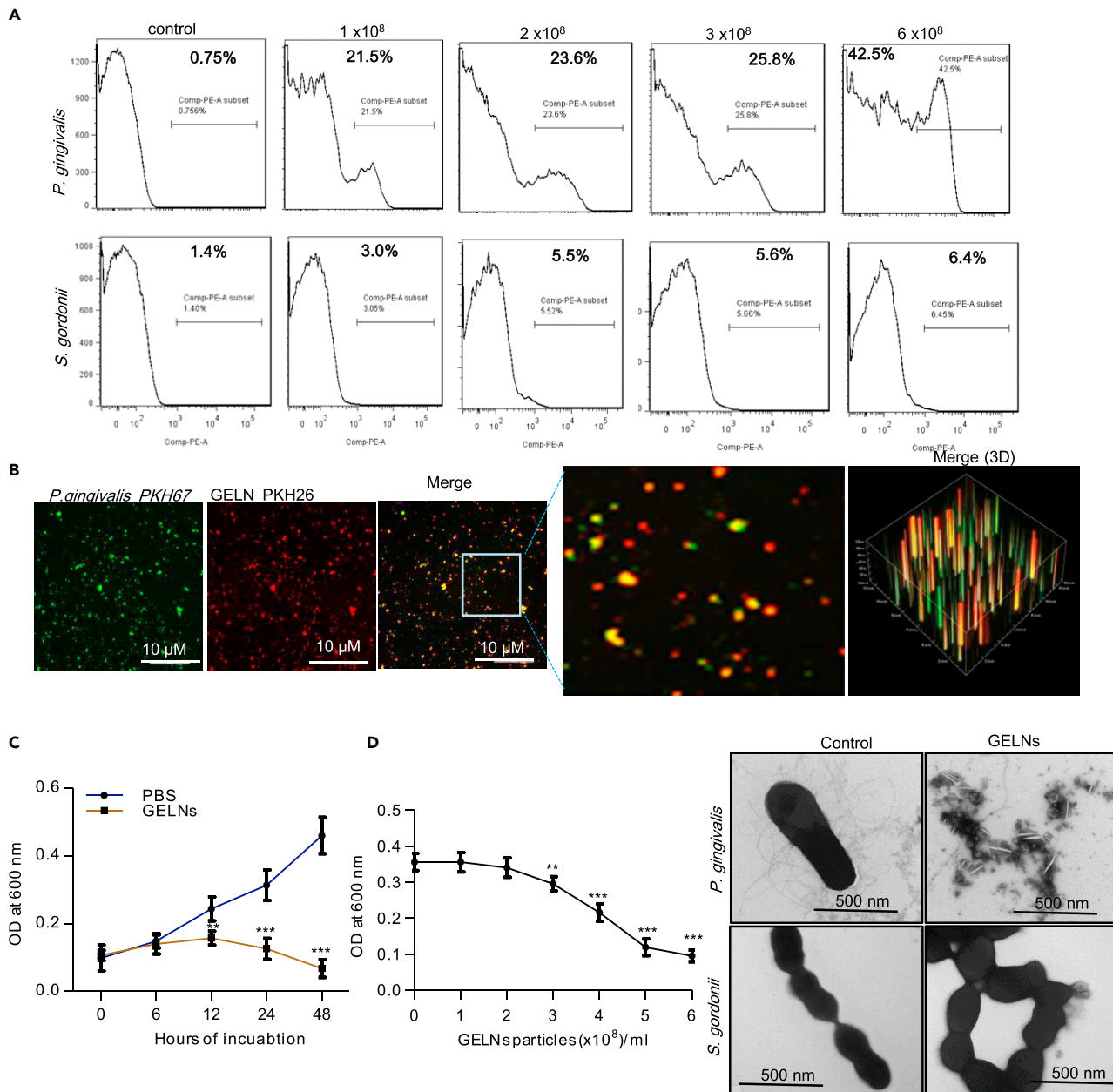
**Figure 1. Ginger Exosome-like Nanoparticles (GELNs) Selectively Inhibit Growth of the Pathogenic *P. gingivalis* but Not the Commensal *S. gordonii***

(A) *P. gingivalis* and *S. gordonii* were incubated with different concentrations (0–6.0 × $10^8$ particles/mL) of PKH26-labeled GELNs for 1 h in an anaerobic chamber. GELN uptake by *P. gingivalis* and *S. gordonii* was quantified by flow cytometry.

(B) *P. gingivalis* and GELNs were labeled with fluorescent dyes PKH67 and PKH26, respectively. Then, *P. gingivalis* and GELNs were incubated at 37°C for 1 h in anaerobic chamber and fluorescence images were taken by confocal microscopy.

(C) *P. gingivalis* was incubated with GELNs (4.0 × $10^8$/mL) for the indicated times. The growth of *P. gingivalis* was determined by measuring optical density at 600 nm.

(D) *P. gingivalis* was treated with different concentrations (0–6 × $10^8$/mL) of GELNs and incubated at 37°C for 24 h. The growth of *P. gingivalis* was determined by measuring optical density at 600 nm. *P. gingivalis* and *S. gordonii* were treated with or without GELNs (6 × $10^8$/mL) for 3 h and negatively stained with ammonium molybdate. The images were taken by transmission electron microscopy.

Results are expressed as mean ± standard deviation from three independent experiments. **p < 0.01, ***p < 0.001 compared with the untreated group using one-way ANOVA with Turkey's Multiple comparison test.
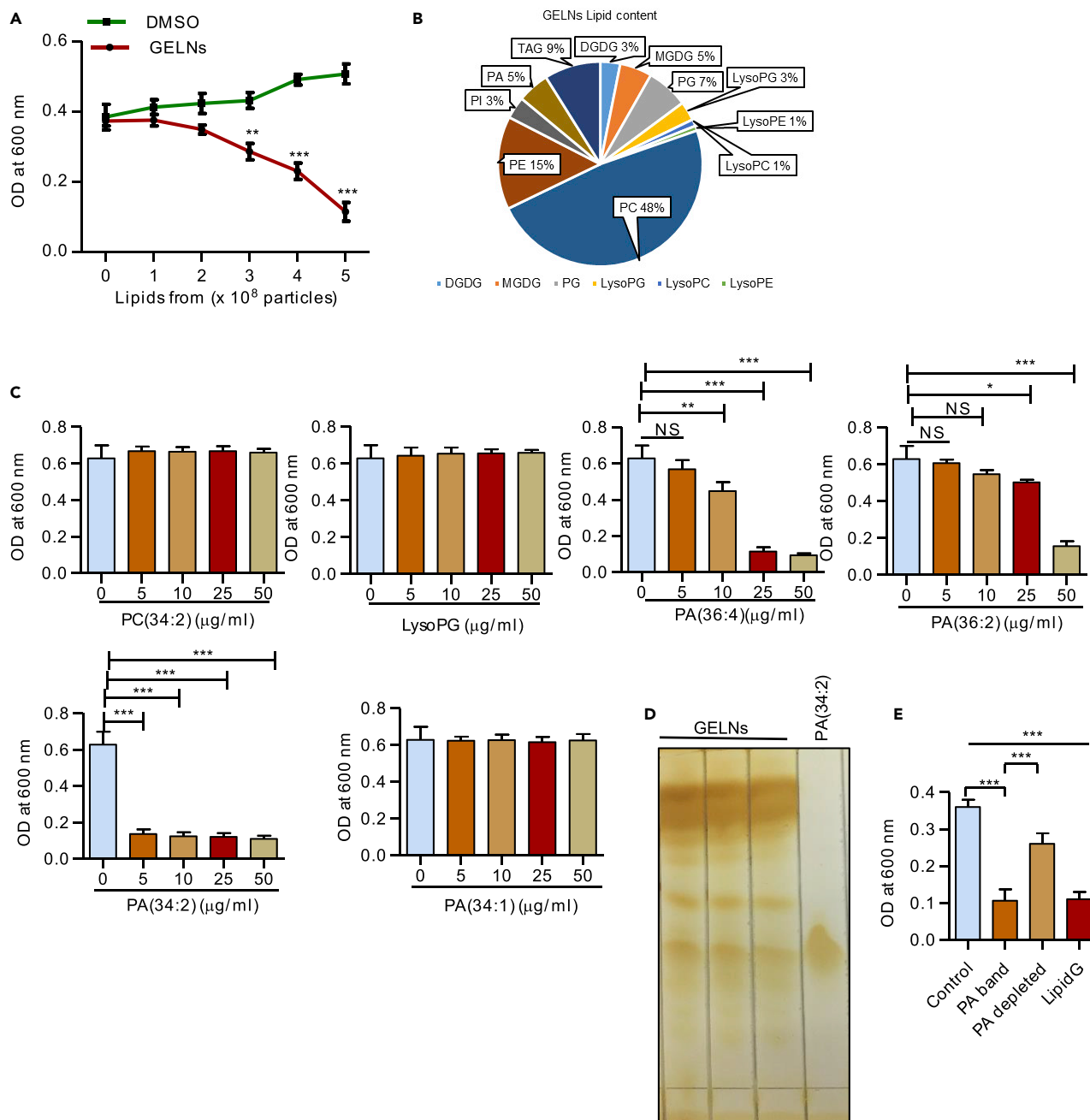
## Figure 2. PA-Containing Lipid of GELNs Inhibits *P. gingivalis* Growth

(A) GELN total lipids (LipidG) isolated from different concentrations of GELNs (0–5.0 × 10$^8$ particles) were reacted with *P. gingivalis* for 24 h in an anaerobic chamber. Bacterial growth was determined by measuring optical density at 600 nm.

(B) Total lipids extracted from GELNs was subjected to mass spectrophotometry for lipid identification. The concentrations of each lipid were calculated as nmol/mg of GELNs.

(C) *P. gingivalis* was treated with different concentrations (0–50 μg/mL) of PC (34:2), LysoPG (18:1), PA (36:4), PA (36:2), PA (34:2), and PA (34:1) for 24 h in an anaerobic chamber. Bacterial growth was determined by measuring optical density at 600 nm.

(D) Total lipids were separated on a silica gel-coated thin-layer chromatography plate.

(E) Depletion of PA lipids in the total GELN lipids (LipidG) by eluting the PA band on a TLC plate and mixing the remaining lipids. *P. gingivalis* was treated with lipids from the PA-containing band, PA depleted and LipidG incubated in anaerobic chamber for 24 h. Bacterial growth was measured at 600 nm.

Results are expressed as mean ± standard deviation from three independent experiments. *p < 0.05, **p < 0.01, ***p < 0.001 compared with an untreated group using a one-way ANOVA with the Turkey's Multiple Comparison Test.

*P. gingivalis* growth. Extracted total lipids from GELNs (5.0 ×10$^8$ particles) were subjected to mass spectrometry analysis. The lipid profile of LipidG is listed in Table S3, and the percentage of each lipid in is presented in Figure 2B. *P. gingivalis* was treated with different concentrations (0–50 μg/mL) of 1-palmitoyl-2-linoleoyl-sn-glycero-3-phosphocholine (PC 34:2), 1-oleoyl-2-hydroxy-sn-glycero-3-phos-pho-(1′-rac-glycerol) (LysoPG 18:1), 1,2-dilinoleoyl-sn-glycero-3-phosphate (PA 36:4), 1,2-dioleoyl-sn-glycero-3-phosphate (PA 36:2), 1-palmitoyl-2-linoleoyl-sn-glycero-3-phosphate (PA 34:2), and 1-palmi-toyl-2-oleoyl-sn-glycero-3-phosphate (PA 34:1). Among these lipids tested, PA (34:2) inhibited *P. gingivalis* growth at a very low concentration (5 μg/mL, 2.5 × 10$^9$ particles have 1 μg of lipid that contains 325.5 nM of PA (34:2) compared with other lipid compounds) (Figure 2C). Next, we sought to determine the role of phosphatidic acid (PA) in the context of GELNs by depletion of PA. Total GELN lipids were extracted and separated by TLC that included a standard PA (34:2) (Figure 2D). The corresponding PA band from the TLC was excised, and the majority of excised lipids is PA (Lipid profile, Table S4); remaining lipids were pooled together as PA-depleted lipids. *P. gingivalis* was incubated with lipidG, the PA-containing band, and the PA-depleted lipids for 24 h. Interestingly, the PA-containing band alone inhibited *P. gingivalis* growth as potently as the total lipids, and in contrast to the PA-depleted lipids, which had min-imal growth inhibition (Figure 2E). Since oxidation may alter the biological activity of the lipids, we further determined the lipid oxidation of GELN lipids before and after TLC extraction. No significant changes in lipid oxidation were observed after TLC extraction (Figure S7). Collectively, these results suggest that PA is the major active molecule in GELN lipids that inhibits *P. gingivalis* growth.

## GELN PA Directly Interacts with HBP35 Protein in *P. gingivalis*, Leading to Inhibition of *P. gingivalis* Growth

We hypothesized that GELN PA lipids interact with an outer membrane protein of *P. gingivalis* that mod-ulates growth. To test this hypothesis, we used Surface Plasmon Resonance (SPR) to identify the *P. gingivalis* proteins that may interact with GELN lipids. We made lipid nanoparticles (Figure S8A) from GELNs PA (34:2) (Figure S8B). In terms of diameter, lipid nanoparticles cover a range between 100 and 500 nm and contain a negligible amount of TAG compared with total lipids derived from GELNs (Figures S8C and S8D). These lipid nanoparticles were immobilized on a LIP-1 sensor. *P. gingivalis* total cell lysates were run over the immobilized nanoparticles as analyte. As shown in Figures 3A–3C, the sensogram of SPR peaks revealed that *P. gingivalis* proteins can interact with lipid nanoparticles with/without depletion of PA lipid and PA (34:2). We eluted the lipid-binding protein from the immobilized nanoparticles by injection of NaOH (200 μM), which causes dissociation of protein from the nanoparticles, and eluted protein samples were subjected to tandem mass spectrometry (MS/MS) for protein identification. Interestingly, we identi-fied several proteins (listed in Table 1) that bound to the GELN lipid nanoparticles and PA (34:2) but not with the PA-depleted lipid nanoparticles. From this result, we identified PA binding with *P. gingivalis* proteins/peptides, including the C-terminal domain of Arg and Lys-gingipain proteases, hemin-binding protein (35 kDa, HBP35), an electron transfer flavoprotein, an esterase, and an outer membrane lipoprotein. These proteins specifically bind with both GELN nanoparticles and PA.

We next wanted to determine which proteins directly interacting with GELNs play an inhibitory role in *P. gingivalis* growth. HBP35 has been shown to be essential for growth of *P. gingivalis* and survival in hemin-depleted conditions (Shibata et al., 2011; Shoji et al., 2010) (Hiratsuka et al., 2010). Therefore, we next examined the interaction of GELNs and its lipids with HBP35. The functional domain of HBP35 is WPRVGQLFIALDQTLGIPGFPTFSVCRME, which plays a critical role in the hemolytic activity of *P. gingivalis* (Hiratsuka et al., 2010). To block the interaction of GELNs with HBP35, we utilized a synthetic peptide (29 amino acids) corresponding to the functional domain. GELNs (4.0 × 10$^8$ particles) were pre-incubated with the functional domain peptide (10 μM), then *P. gingivalis* was reacted with the GELNs and growth was measured. Interestingly, *P. gingivalis* growth was not affected by GELNs pre-incubated with HBP35 peptide (Figure 4A). Similarly, LipidG made from total lipid of 4.0 and 6.0 × 10$^8$ GELNs (Fig-ure 4B) and PA (34:2) (Figure 4C) were pre-incubated with HBP35 synthetic peptide and treated with *P. gingivalis*. The synthetic peptide significantly blocked GELN lipids and PA-mediated inhibition of *P. gingivalis* growth (Figures 4B and 4C). To test whether the HBP35 synthetic peptide directly binds with PA (34:2) and PA (34:1) of GELN lipids, we again utilized SPR. Lipid nanoparticles from GELN total lipids, PA-depleted lipid, PA (34:2), and PA (34:1) were immobilized on the LIP-1 sensor. The HBP35 synthetic peptide and a non-specific peptide were used as analyte. The SPR sensogram peaks show that the HBP35 synthetic peptide directly interacts with GELNs and PA (34:2) nanoparticles but not with PA-depleted lipid nanoparticles and PA (34:1) nanoparticles (Figures 4D–4G). This result indicates that
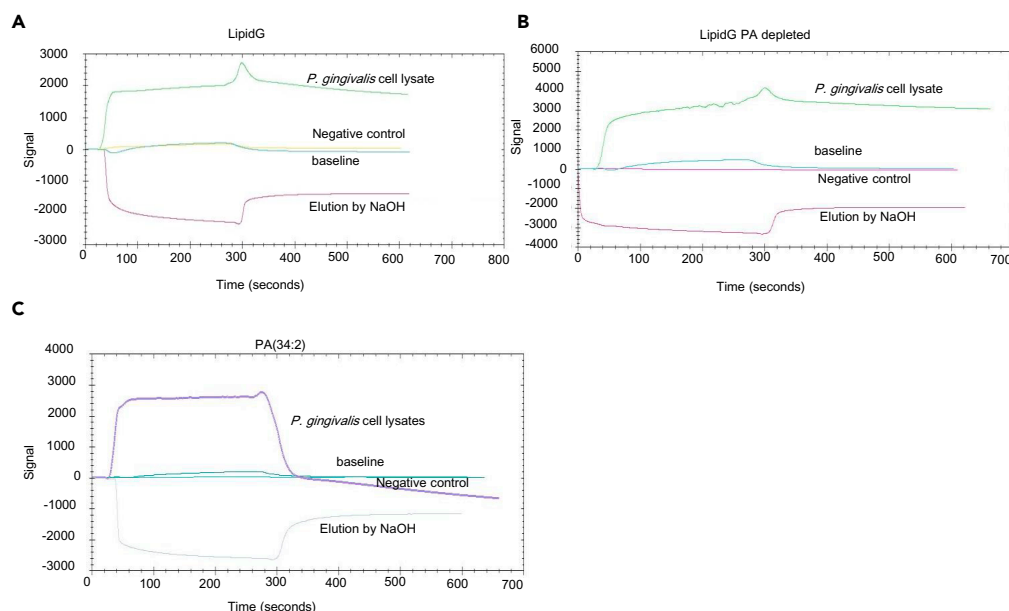
**Figure 3. Identification of PA-Binding Proteins in *P. gingivalis***

Lipid nanoparticles were prepared from LipidG, PA-depleted GELN lipids, and PA (34:2), and these lipid nanoparticles were immobilized on a LIP-1 sensor. Total *P. gingivalis* cell lysates were used as analyte as described in the Transparent Methods. The lipid-protein interaction was determined by SPR sensograms.

(A) Sensogram of GELNs lipid nanoparticles.

(B and C) (B) Sensogram of PA-depleted GELN lipid nanoparticles and (C) Sensogram of PA (34:2) lipid nanoparticles. Protein bound with lipid nanoparticles was eluted by NaOH (200 μM), and the fraction was collected for MS/MS analysis for protein identification. The lipid-binding proteins in *P. gingivalis* are listed in Table 1.

the degree of unsaturation of PA plays a critical role in GELN-mediated interaction with HBP35. In addition to using SPR, we further confirmed PA binding to HBP35 by a pull-down assay. PA (34:2) nanoparticles were fluorescently labeled with PKH26 (PE channel) and incubated with biotin-HBP35 peptide for 2 h. The lipid-peptide complex was pulled down by streptavidin beads, and the complex was washed thoroughly. The presence of PA (34:2) in the complex was confirmed by flow cytometry (Figure 4H, top panel). The number of lipid nanoparticles (Figure 4H, bottom, left panel) and fluorescent intensity (Figure 4H, bottom, right panel), including GELNs with/without depletion of PA, PA band from GELN, and PA (34:2) in the complex was determined. The results generated from all three independent assays demonstrated that PA lipid binds to HBP35. We further tested inhibition of GELN uptake by HBP35 peptide. *P. gingivalis* was fluorescently labeled with PKH67 (green), whereas GELNs and lipid nanoparticles were labeled with PKH26 (red). GELNs and GELN lipid nanoparticles were pre-incubated with HBP35 peptide (10 μM) and then reacted with *P. gingivalis* for 1 h at 37°C. *P. gingivalis* uptake of GELNs and lipid nanoparticles was visualized by confocal microscopy (Figure 4I) and quantified by flow cytometry (Figure 4J). Pre-incubation of synthetic peptide with GELNs and lipid nanoparticles significantly decreased *P. gingivalis* uptake of GELNs and lipid nanoparticles. HBP35-dependent GELN uptake by *P. gingivalis* was further demonstrated by deletion of the gene encoding HBP35 in *P. gingivalis*. The wild-type and HBP35 mutant of *P. gingivalis* were incubated with PKH26-labeled GELNs for 1 h at 37°C, and GELN uptake was quantified by flow cytometry. As shown in Figure 4K, the *HBP35* mutant had a significantly decreased uptake of GLENs. Furthermore, the mutation of the gene HPB35 in *P. gingivalis* led to less inhibition of its growth by GELNs compared with wild-type *P. gingivalis* (Figure 4L). Taken together, these results suggest that the lipid moiety of GELNs, specifically PA (34:2), interacts with HBP35 on the outer membrane of *P. gingivalis*, and this interaction followed by lipid uptake leads to inhibition of bacterial growth.

## GELN miRNAs and Lipid PA (34:2) Inhibit the Virulence Activity of Gingipain and Type IX Secretion System of *P. gingivalis*

Besides growth, there are many specific virulence factors that which contribute to the pathogenicity of *P. gingivalis* (Lamont et al., 2018). GELNs are complex nanoparticles that could interact with a multiple

| Identified Proteins | Gene Symbol | Accession Number | Quantitative Value (iBAQ) | | |
|---|---|---|---|---|---|
| | | | GELN Lipid Nanoparticles | PA Depleted GELN | PA (34:2) Lipid Nanoparticles |
| CTD of Arg- and Lys-gingipain proteinase | rgpA | B2RHG9_PORG3 | 8,269,700 | 0 | 5.49E+07 |
| Uncharacterized protein | PGN_1182 | B2RK06_PORG3 | 1,974,600 | 0 | 4,816,600 |
| Exo-glucosaminidase LytG muramidase | lytG | B2RME7_PORG3 | 1,870,800 | 0 | 628,530 |
| 35 kDa hemin-binding protein | HBP35 | B2RII3_PORG3 | 540,420 | 0 | 1.11E+07 |
| Probable transcriptional regulator | asnC | B2RK48_PORG3 | 428,670 | 0 | 0 |
| Electron transfer flavoprotein beta subunit | carD | B2RJZ7_PORG3 | 280,750 | 0 | 3,750,900 |
| META domain lipoprotein implicated in motility | PGN_0740 | B2RIR4_PORG3 | 215,870 | 0 | 1,347,800 |
| Methylmalonyl-CoA decarboxylase-α subunit | pccB | B2RI24_PORG3 | 195,390 | 0 | 2,510,400 |
| 30S ribosomal protein S4 | rpsD | RS4_PORG3 | 190,850 | 0 | 2,002,700 |
| Oxygen-insensitive NADPH nitroreductase | rdxA | B2RIT9_PORG3 | 80,440 | 0 | 0 |
| Lys-gingipain protease | kgp | B2RMI8_PORG3 | 72,555 | 0 | 0 |
| Esterase | estD | B2RM02_PORG3 | 38,153 | 0 | 1,953,400 |
| Outer membrane lipoprotein 42 kDa antigen PG33 | ompA | B2RKC0_PORG3 | 36,170 | 0 | 0 |
| Uncharacterized protein | PGN_1697 | B2RLH1_PORG3 | 34,827 | 0 | 0 |
| Protein translocase SecA | secA | SECA_PORG3 | 30,589 | 0 | 0 |
| NAD-dependent 4-hydroxybutyrate dehydrogenase | adh | B2RIP8_PORG3 | 13,268 | 0 | 2,250,200 |
| L-erythro-35-diaminohexanoate dehydrogenase | kdd | B2RJY9_PORG3 | 10,490 | 0 | 1,263,500 |
| Chaperone protein DnaK | dnaK | DNAK_PORG3 | 6,316.60 | 0 | 23,177 |
| Long-chain-fatty-acid-CoA ligase | fadD | B2RK69_PORG3 | 4,928.30 | 0 | 0 |

**Table 1. PA-Binding Protein in *P. gingivalis*.**

of *P. gingivalis* virulence factors in addition to HBP35. To search for *P. gingivalis* factors that could interact with GELNs, biotin-labeled GELNs were incubated with *P. gingivalis* total cell lysates. After pull-down with streptavidin beads, the *P. gingivalis* factors that bind with GELNs were separated by SDS-PAGE, and analyzed by MS/MS (Figures 5A and 5B). The GELN-binding proteins which included HBP35, lysine and arginine gingipain, hemagglutinin (HagA), outer membrane protein A (OmpA), and type IX secretion system (T9SS) were identified (Table S5). Interestingly, we identified using two independent assays that GELN interacts with HBP35: the biotin pull-down and SPR assays.

As an asaccharolytic organism *P. gingivalis* is highly proteolytic and the arginine- and lysine-specific gingipain are responsible for nearly 85% of the total proteolytic activity (Potempa et al., 2003). Gingipain are involved in a variety of pathogenic functions, including colonization, nutrition, and neutralization of host defenses, and contribute to extensive periodontal tissue destruction. Both the lysine-specific (Kgp) and arginine-specific (RgpA and RgpB) gingipain are also involved in the accumulation of hemin derivatives of the cell surface giving rise to black pigmentation of *P. gingivalis* colonies on blood agar (Lasica et al., 2016) (Smalley and Olczak, 2017). GELN treatment inhibited the formation of black-pigmented colonies of *P. gingivalis* (Figure 5C). This result was further supported by the finding that activity of both Rgp and Kgp was significantly decreased in *P. gingivalis* treated with GELNs (Figure 5D). GELN lipids, PA (34:2) (Figure 5E), and GELNs aly-miR159a (Figure 5F) all contributed to the inhibition of Rgp and Kgp activities.
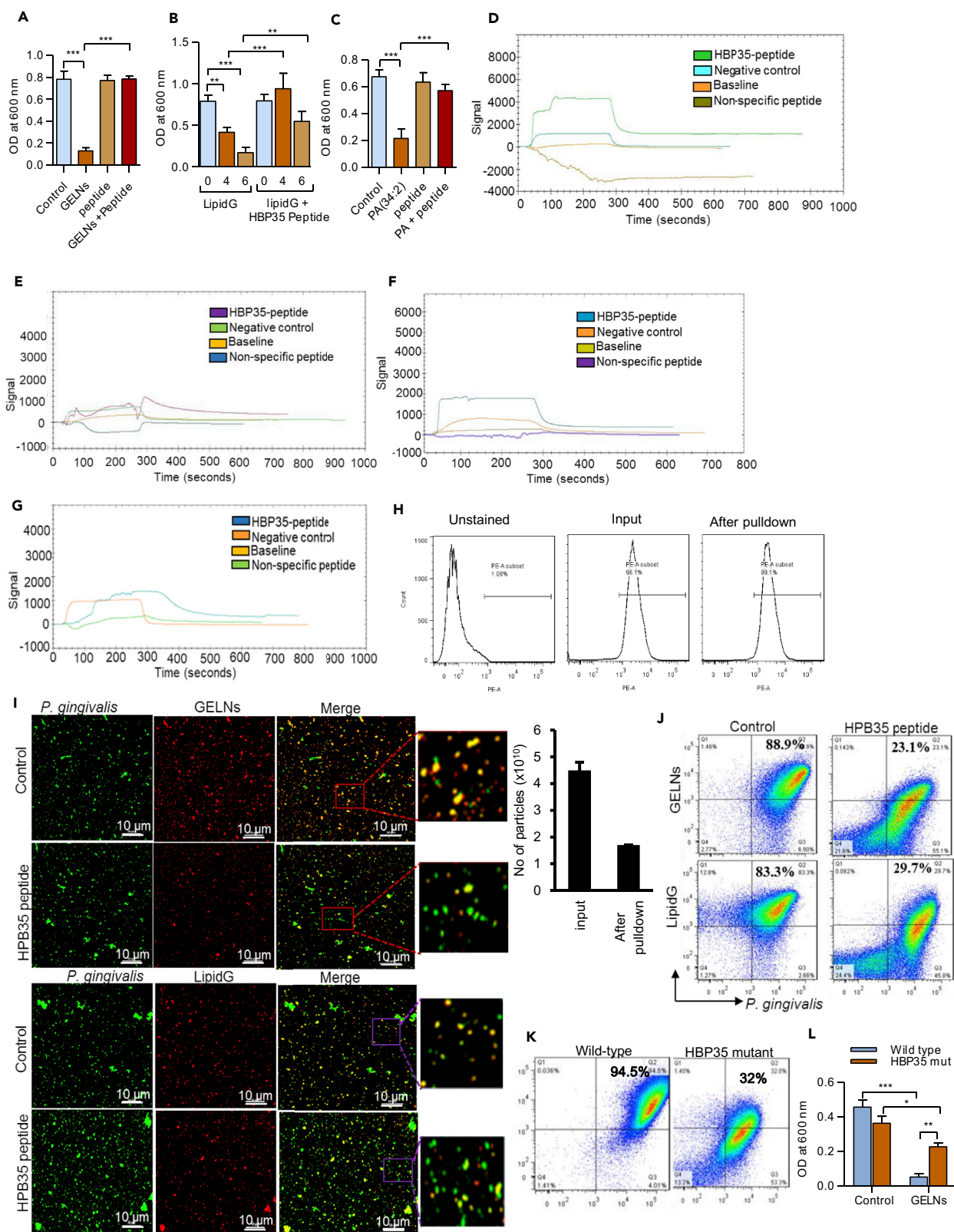
**Figure 4. GELN Lipids Bind to Hemin-Binding Protein 35 (HBP35) on the Outer Membrane of *P. gingivalis* and Inhibit Its Growth**

(A–E) (A–C) A synthetic peptide representing the functional domain of HBP35 WPRVGQLFIALDQTLGIPGFPTFSVCRME (10 μM) was pre-incubated with GELNs (4.0 × 10$^8$ particles), LipidG (4.0–6.0 × 10$^8$ particles), and 5 μg of PA (34:2) for 1 h at 37°C. The pre-treated GELNs and lipids were reacted with *P. gingivalis* for 24 h in anaerobic chamber, and growth of *P. gingivalis* was measured at 600 nm. Determination of direct binding of PA with HBP35 by surface plasmon resonance. Lipid nanoparticles were made from (D) LipidG (E) PA depleted GELN lipids.

(F and G) (F) PA (34:2) and (G) PA (34:1). These lipid nanoparticles were immobilized on a LIP-1 sensor, and HBP35 synthetic peptide was used as an analyte and non-specific peptide used as a negative control. The lipid-protein interaction was determined by SPR sensograms.

(H) Lipid nanoparticles were made from GELN lipids, PA-depleted GELNs, the PA-containing band, and PA (34:2). These nanoparticles were labeled with PKH26 red fluorescent dye and incubated with biotin-HBP35 peptide for 2 h at room temperature with rotation. The lipid nanoparticles and peptide complex were precipitated with streptavidin beads. After washing with PBS, the presence of lipid nanoparticles in the complex was confirmed by flow cytometry. The number of lipid nanoparticles in the complex was measured using a NanoSight 300, and the quantity of lipid nanoparticles was determined by fluorescence intensity as described in Transparent Methods.

(I) *P. gingivalis* was labeled with PKH67 (Green), and GELNs and GELN lipid nanoparticles were labeled with PKH26 (Red). The labeled particles were pre-incubated with synthetic peptide of HBP35 (10 μM) for 1 h at 37°C. Then, particles were treated with labeled *P. gingivalis* for 1 h at 37°C in an anaerobic chamber. Uptake of particles by *P. gingivalis* were visualized by confocal microscopy.

(J) *P. gingivalis* uptake of particles were quantified by flow cytometry.

(K) *P. gingivalis* wild-type and Δ*hbp35* mutant were labeled with PKH67, and GELNs were labeled with PKH26. GELNs were reacted with *P. gingivalis* for 1 h at 37°C in an anaerobic chamber. *P. gingivalis* and Δ*hbp35* mutant uptake of particles was quantified by flow cytometry.

(L) *P. gingivalis* wild-type and *hbp35* mutant was reacted with GELNs for 24 h in an anaerobic chamber. Bacterial growth was determined by measuring optical density at 600 nm.

Results are expressed as mean ± standard deviation from three independent experiments. *p < 0.05, **p < 0.01, ***p < 0.001 compared with an untreated group using a one-way ANOVA with the Turkey's Multiple Comparison Test.

We also examined the expression of genes encoding other *P. gingivalis* proteins that have the potential to contribute to the pathophysiology of the organism. GELNs strongly inhibited expression of mRNA encoding the AraC transcription factor; HagA, hemagglutinin; OmpA, outer membrane protein A; and the RodA, rod shape determining protein (Figure 5G). Furthermore, GELN aly-miR159a, gma-miR166u/p differentially regulated mRNA expression of AraC, HagA, OmpA, and RodA (Figure 5H). In addition, we found an aly-miR159a-3p-binding site in *hagA* (PGN_1733) and *araC* (PGN_0082), and gma-166p has a potential binding site in *ompA* (PGN_0299) (Figure S9). Indeed, miRNAs derived from GELNs have putative binding sites in several *P. gingivalis* genes, indicating the potential for broadly based inhibition of *P. gingivalis* function. Additionally, lipids derived from GELNs and PA (34:2) inhibited *araC*, *hagA*, *ompA*, and *rodA* mRNA expression (Figure 5I). Collectively, these results indicate that GELN-derived lipids and miRNAs target several virulence genes expressed in *P. gingivalis*.

The translocation of gingipain to the bacterial surface requires the type IX secretion system (T9SS) (de Diego et al., 2016). T9SS also secrete a variety of other potential virulence factors that possess a conserved C-terminal domain (Lasica et al., 2017). Hence, we examined the role of GELNs and GELN lipids and miRNAs in modulating the expression of genes related to the T9SS. *P. gingivalis* was treated with GELNs (4.0 × 10$^8$ particles/mL) and GELN lipids derived from 4.0 × 10$^8$ particles, or 5 μg of PA (34:2) for 6 h miRNAs aly-miR159a, gma-miR166u, and gma-miR166p were transduced individually into *P. gingivalis* and incubated for 24 h. The expression of the T9SS family of genes (Vincent et al., 2017) including *porK*, *porL*, *porN*, *porP*, *porQ*, *porT*, *porV*, *porW*, *porX*, *porY*, and *sov* was quantified using RT-qPCR. GELNs and GELN total lipids significantly inhibited the expression of 11 of the 12 T9SS family of genes compared with the control (Figures 6A and 6B). In addition, PA (34:2) and miRNAs differentially modulated the expression of the T9SS family of genes (Figures 6B and 6C). Furthermore, we found aly-miR159a-3p has a binding site in the T9SS C-terminal target domain containing protein (PGN_0152) (Figure S9). Taken together, GELNs and total lipids derived from GELNs inhibit expression of the T9SS family of genes. GELN miRNAs and PA (34:2) preferentially inhibited expression of some of the T9SS family of genes, which can be predicted to impact the ability of the organism to secrete important virulence factors.

### GELNs Inhibits *P. gingivalis* Attachment to and Invasion in Oral Epithelial Cells

The early stages of *P. gingivalis* colonization involve attachment and invasion of gingival epithelial cells (Lamont et al., 1995); therefore, we determined whether GELNs have an effect on these processes. *P. gingivalis* was treated with GELNs (4 ×10$^8$ particles/mL) for 3 h, and then gingival epithelial cells (human telomerase immortalized gingival keratinocytes [TIGKs]) were infected with *P. gingivalis* (MOI 10) for 1 h. Visualization of *P. gingivalis* attachment to TIGKs by confocal microscopy showed that GELN treatment significantly decreased the level of *P. gingivalis* binding (Figure 7A). Consistent with this, when attachment

A

M   1   2

1. Total cell lysate
2. GELN-biotin pulldown

B

RT: 0.00 - 60.00

Relative Abundance

C

PBS

GELNs

D



E



F



G

*AraC*

*HA*

*OMP*

*RodA*

H

*AraC*

*HA*

*OMP*

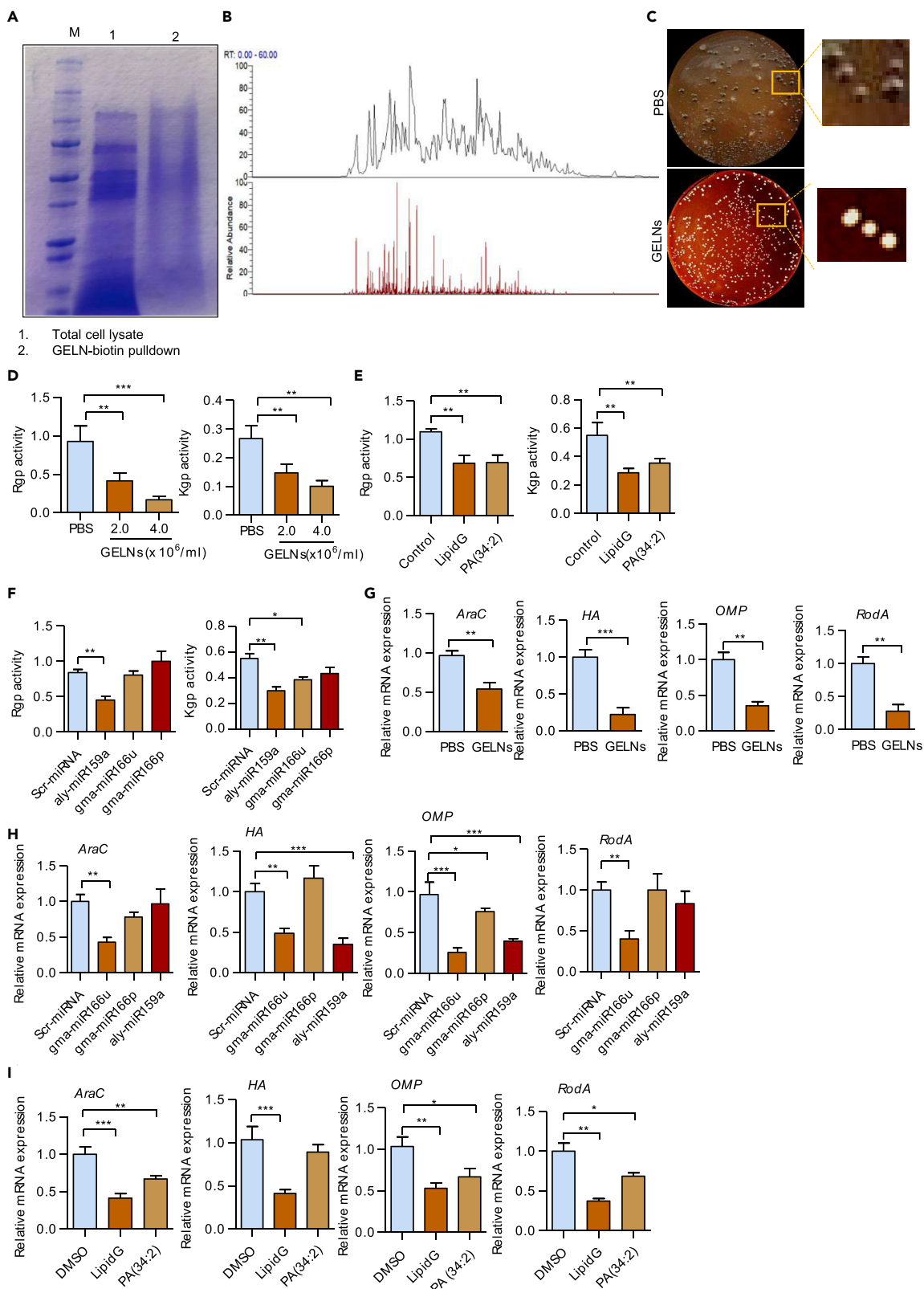*RodA*

I

*AraC*

*HA*

*OMP*

*RodA*

**Figure 5. Identification of GELN-Binding Proteins in *P. gingivalis***

GELNs were labeled with biotin and incubated with total cell lysates of *P. gingivalis* for 1 h at room temperature. GELN-binding proteins were pulled down by streptavidin-conjugated beads.

(A) Protein was separated by SDS PAGE.

(B) Pull-down proteins were subjected to MS/MS analysis.

(C) *P. gingivalis* was incubated with GELNs (4.0 × 10$^8$ particles/mL) for 6 h in an anaerobic chamber; the bacteria was spread on blood agar plates and incubated anaerobically for 1 week.

(D) *P. gingivalis* was incubated with different concentrations (2.0 or 4.0 × 10$^8$ particles/mL) of GELNs for 6 h. *P. gingivalis* was lysed with Bugbuster lysis reagent, and gingipain activities were measured using specific substrates for Arg-specific protease (Rgp) and Lys-specific protease (Kgp).

(E) *P. gingivalis* was treated with total lipids derived from GELNs and PA (34:2) for 6 h. Gingipain activity was measured in *P. gingivalis* cell lysates.

(F) *P. gingivalis* was transduced with scrambled miRNA, aly-miR159a-3p, gma-miR166u, or gma-miR166p for 24 h and gingipain activity measured in total cell lysates.

(G) *P. gingivalis* was treated with GELNs (4 × 10$^8$ particles/mL) for 6 h.

(H) Transduced with scrambled miRNA, aly-miR159a, gma-miR166u, or gma-miR166p for 24 h. Expression of mRNA for *araC*, *hagA*, and *rodA* was determined by RT-qPCR.

(I) *P. gingivalis* was treated with total lipids derived from GELNs (4 × 10$^8$ particles) or 5 μg of PA (34:2) for 6 h. Expression of mRNA for *araC*, *hagA*, and *rodA* was determined by RT-qPCR.

Results are expressed as mean ± standard deviation from three independent experiments. *p < 0.05, **p < 0.01, ***p < 0.001 compared with untreated group using one-way ANOVA with Turkey's Multiple Comparison Test.

of *P. gingivalis* to TIGK cells was determined by enzyme-linked immunosorbent assay (ELISA), GELN treatment significantly decreased the surface binding of *P. gingivalis* to TIGK cells (Figure 7B).

The FimA component fimbriae are required for attachment of *P. gingivalis* to oral epithelial cells (Tribble and Lamont, 2010). Therefore, we next sought to determine the effect of GELNs on expression of FimA, as well as on expression of the Mfa1 component fimbriae. As presented in Figures 7C and 7D, expression FimA at both mRNA and protein levels was decreased by GELN treatment. However, GELNs did not change expression of Mfa1. Attachment of *P. gingivalis* to epithelial surfaces can also induce internalization of the organism, which can survive intracellularly. Pre-treatment of *P. gingivalis* with different concentrations of GELNs (0–6.0 ×10$^8$ particles/mL) for 3 h decreased intracellular invasion of TIGKs in an antibiotic protection assay (Figure 7E). After 24 h within the TIGKs, quantitation of intracellular *P. gingivalis* by qPCR analysis using 16S rRNA expression showed that GELNs significantly inhibit intracellular proliferation (Figure 7F). These results indicate that GELNs significantly inhibit attachment and invasion of *P. gingivalis* into oral epithelial cells.

Next, we determined which GELN factors contribute to the inhibition of the attachment and invasion of *P. gingivalis* in oral epithelial cells. We pretreated *P. gingivalis* with GELN-derived total lipids (from 4.0 × 10$^8$ GELNs) and 50 nM of PA (34:2), which is equivalent to lipids extracted from 4.0 × 10$^8$ GELNs for 3 h. Under these conditions *P. gingivalis* was not killed; however, there was a significant inhibition of attachment to TIGK cells (Figure 7G). Furthermore, *P. gingivalis* was treated with the same concentration of lipids for 6 h and FimA expression was determined by western blot and RT-qPCR analysis. FimA expression was decreased significantly (p = 0.002) in both LipidG- and PA (34:2)-treated *P. gingivalis* (Figures 7H and 7I). Furthermore, we next examined the effect of GELN total lipids and PA (34:2) on *P. gingivalis* invasion and proliferation in TIGK cells. A significant decrease in *P. gingivalis* invasion and proliferation was observed with both GELN total lipids and PA-treated *P. gingivalis* (Figures 7J and 7K). Collectively, these results suggest that GELN PA (34:2) inhibits the growth, attachment, and invasion of *P. gingivalis*.

To test whether GELN miRNAs play an inhibitory role in attachment and invasion of *P. gingivalis*, we transduced miRNAs gma-miR166u, gma-miR166p, or aly-miR159a into *P. gingivalis* and used scrambled miRNA as a control. Among these three miRNAs tested, aly-miR159a significantly decreased the attachment of *P. gingivalis* to TIGK cells and gma-miR166u and gma-166p moderately inhibited attachment (Figure 7L). Next, we determined the effect of these miRNAs on *P. gingivalis* invasion (Figure 7M) and proliferation (Figure 7N). As with attachment, inhibition of invasion by aly-miR159a was most pronounced (Figure 7M) and all of the miRNAs inhibited proliferation (Figure 7N). Collectively, these results suggest that GELNs and total lipids derived from GELNs, as well as constituent miRNAs, can impede colonization of *P. gingivalis* by antagonizing epithelial cell attachment and invasion.

## GELNs Inhibit *P. gingivalis*-Induced Bone Loss in an In Vivo Mouse Model

Consistent with its role as a periodontal pathogen, *P. gingivalis* can induce alveolar bone loss in rodent models (Baker et al., 2000). *P. gingivalis*, along with other pathogenic bacteria in the oral cavity, reside
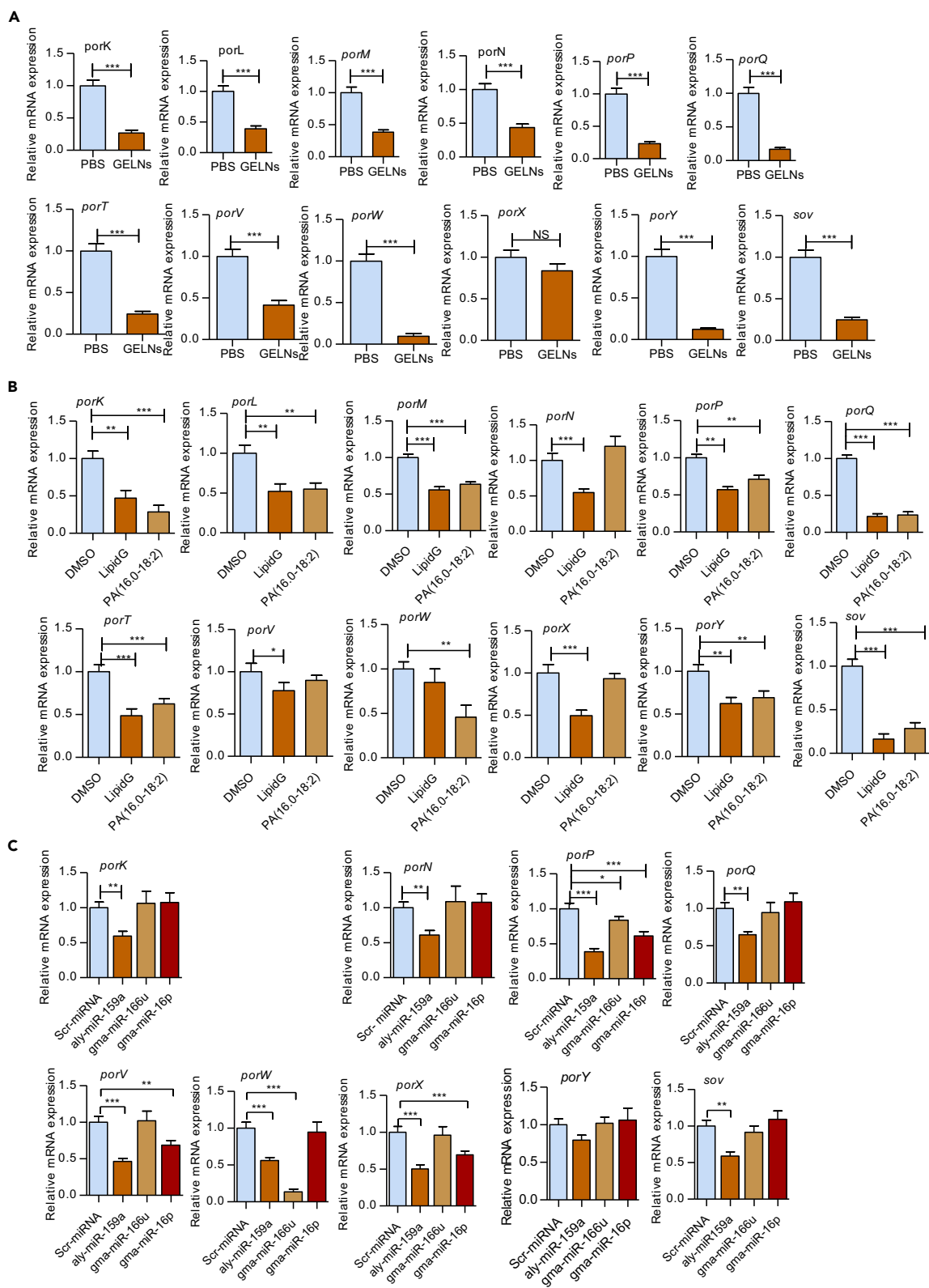
**Figure 6. GELNs Inhibit T9SS mRNA Expression in *P. gingivalis***

(A) *P. gingivalis* treated with GELNs ($4 \times 10^8$ particles/mL).

(B) *P. gingivalis* treated with lipids extracted from GELNs ($4 \times 10^8$ particles) or 5 μg of PA (34:2) for 6 h.

(C) *P. gingivalis* was transduced with scrambled miRNA, aly-miR159a, gma-miR166u, or gma-miR166p for 24 h T9SS family mRNA expression was measured by RT-qPCR.

Results are expressed as mean ± standard deviation from three independent experiments. *p < 0.05, **p < 0.01, ***p < 0.001 compared with untreated group using the one-way ANOVA with Turkey's Multiple Comparison Test and Student's t test.

primarily in biofilm structures, which contribute to the alveolar bone loss. GELNs dose dependently decreased *P. gingivalis* biofilm formation *in vitro* (Figure S10). Therefore, we next wanted to test the effect of GELNs on *P. gingivalis*-induced alveolar bone loss. To confirm uptake of GELNs by *P. gingivalis* in the mouse oral cavity we inoculated fluorescent labeled (PKH67) *P. gingivalis* followed by fluorescent labeled (PKH26) GELNs. After 1 h incubation, the oral cavity was washed with PBS. As shown in Figures 8A and 8B, flow cytometry and confocal microscopy analyses of this PBS wash showed that *P. gingivalis* in the mouse oral cavity can take up GELNs. Next, the ability of GELNs to prevent/inhibit bone loss was examined. *P. gingivalis* was inoculated into the murine oral cavity every 2 days for a period of 10 days, and GELNs were given in drinking water *ad libitum* continuously until the end of the experiment. After 3 weeks, the colonization of *P. gingivalis* in the oral cavity was determined by qPCR. Oral samples were collected along the gingiva of the upper molars using a 15-cm sterile polyester-tipped applicator, and total genomic DNA was purified and amplified by qPCR with primers to 16 S rRNA. Numbers of *P. gingivalis* were calculated by comparison with a standard curve derived from known amounts of *P. gingivalis*. As shown in Figure 8C, the number of *P. gingivalis* in the oral cavity was significantly decreased with GELN treatment. This result indicates that GELN treatment given in drinking water had significant inhibition of colonization of *P. gingivalis*. In addition, the presence of *P. gingivalis* in the oral tissue was confirmed by confocal microscopy. It showed that *P. gingivalis* in the oral tissue was decreased in GELNs treated group compared with *P. gingivalis* alone infected tissue (Figure 8D). Furthermore, the *in vivo* uptake of GELNs by *P. gingivalis* was determined by confocal microscopy (Figure 8E). After 48 days, the mice were sacrificed and μCT analysis was used to determine alveolar bone loss by measuring the distance from the cementoenamel junction to the alveolar bone crest. In addition, bone volume was measured. A region of interest (ROI) was drawn manually on the axial planes, between the medial root surface of the first molar and distal root surface of the third molar. A three-dimensional image was generated from the ROI. All root volumes were excluded from the ROI to calculate the total volume (TV). The bone volume fraction (BV/TV) was calculated for each sample. GELNs significantly decreased *P. gingivalis*-induced bone loss, demonstrating that GELNs can inhibit *P. gingivalis* pathogenicity *in vivo* (Figures 8F–8H). Interestingly, GELNs alone significantly increased the bone density of alveolar bone compared with the sham condition (Figure 8H). Next, we sought to determine the effect of GELNs on osteoclast differentiation and osteoblast function in infected mice. GELNs treatment significantly decreased TRAP$^+$ osteoclast number in *P. gingivalis*-infected mice compared with untreated mice (Figure 8I). Osteoblast cells were stained by RUNX2 expression and immunohistochemistry. As shown in Figure 8I, RUNX2 expression was significantly decreased in *P. gingivalis*-infected oral tissue sections, whereas RUNX2 expression was significantly increased by GELN treatment in *P. gingivalis*-infected mice. These results suggest that GELNs differentially regulate osteoclasts and osteoblasts in *P. gingivalis*-infected mice. Furthermore, we screened the cytokine profile in mouse plasma modulated by *P. gingivalis* and GELNs. Cytokine array analysis revealed that GELNs significantly decreased *P. gingivalis* induction of pro-inflammatory cytokines and documented bone resorptive cytokines, such as TNF-α, IL-1α, IL-1β, INF-γ, IL-6, IL-13, and IL-22 (Figure S11). These cytokines play an important role in recruiting inflammatory Th17 T cells and macrophages into periodontal tissues, leading to bone loss (Baker et al., 1999) (Lam et al., 2014; Tzach-Nahman et al., 2017; Zhuang et al., 2018). Next, we investigated the effect of GELNs on T cell, macrophage, and leukocyte recruitment by using immunofluorescent labeled CD3, F4/80, and CD45 antibodies to detect T cells, macrophages, and leukocytes, respectively. As shown in Figures 8J–8L, *P. gingivalis* infection enhanced infiltration of T cells, macrophages, and leukocytes in periodontal tissues and this infiltration was decreased significantly by GELNs. Furthermore, qPCR analysis showed that GELNs significantly decreased *P. gingivalis*-induced expression of mRNA for the inflammatory and bone resorptive cytokines IL-1β, IL-6, IL-8, and TNF-α in oral tissue (Figure 8M). Also, histology of oral sections showed increased cellular infiltration in the periodontal ligament region in *P. gingivalis*-infected mice compared with control, and this cellular infiltration was significantly decreased in GELN-treated mice (Figure 8N). Taken together, these results suggest that GELNs can target *P. gingivalis* and inhibit the expression of virulence factors and thereby decrease alveolar bone loss and inflammation induced by the organism *in vivo*.
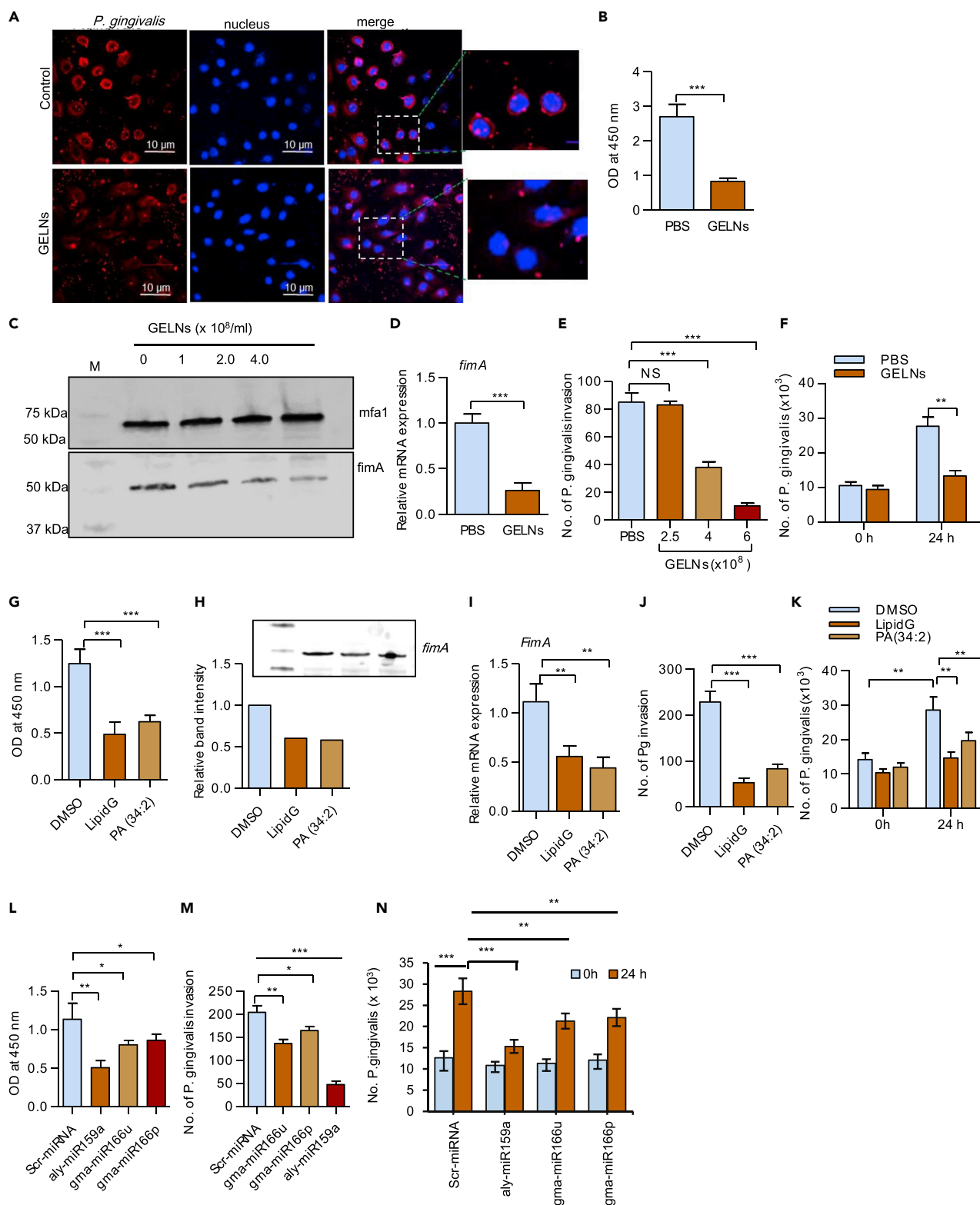
**Figure 7. GELNs Inhibit *P. gingivalis* Attachment, Invasion, and Proliferation in Oral Epithelial Cells**

(A) *P. gingivalis* was treated with or without GELNs ($4.0 \times 10^8$ particles/mL) for 3 h and reacted with TIGK cells at an MOI of 10 for 1 h. *P. gingivalis* was stained with whole-cell antibody, and the nucleus was stained with DAPI.

### Figure 7. *Continued*

(B) *P. gingivalis* was treated with or without GELNs (4.0 × 10$^8$ particles/mL) for 3 h and reacted with TIGK cells at an MOI of 10 for 1 h. Binding was determined by ELISA.

(C) *P. gingivalis* was treated with or without GELNs (0–4.0 × 10$^8$ particles/mL) for 6 h, and total cell lysates were subjected to western blotting with the antibodies as indicated.

(D) *P. gingivalis* was treated with or without GELNs (4.0 × 10$^8$ particles/mL) for 24 h, and *fimA* mRNA expression was determined by RT-qPCR.

(E) *P. gingivalis* was treated with different concentrations of GELNs (0–4.0 × 10$^8$ particles/mL) for 3 h and invasion of TIGK cells determined by an antibiotic protection assay as described in the Transparent Methods section. The results are expressed as number of *P. gingivalis* invasion into TIGK cells.

(F) *P. gingivalis* was treated with or without GELNs (4.0 × 0$^8$ particles/mL) and infected into TIGK cells at an MOI of 10. After further culturing for 24 h, numbers of intracellular bacteria were determined by qPCR.

(G) *P. gingivalis* was treated with or without GELN (from 6 ×10$^8$ particles/mL) derived LipidG or PA (34:2) (5 μg/mL) and surface attachment to TIGK cells measured.

(H) *P. gingivalis* was treated with or without LipidG (from 6 ×10$^8$ particles/mL) or PA (34:2) (5 μg/mL) for 6 h, and cell lysates were examined by western blotting with FimA antibodies.

(I–K) (I) *P. gingivalis* was treated with or without LipidG (from 6 ×10$^8$ particles/mL) or PA (34:2) (5 μg/mL) and *fimA* mRNA determined by RT-qPCR (J) *P. gingivalis* invasion into oral epithelial cells and (K) *P. gingivalis* proliferation in oral epithelial cells as described in the Transparent Methods.

(L) *P. gingivalis* was transduced with miRNA from GELN aly-miR159a, gma-miR166u, gma-miR166p, or non-specific scrambled miRNA for 24 h and attachment to TIGK cells measured by ELISA.

(M and N) (M) *P. gingivalis* invasion into oral epithelial cells and (N) *P. gingivalis* proliferation in oral epithelial cells were determined as described in the Transparent Methods.

Results are expressed as mean ± standard deviation from three independent experiments. *p < 0.05, **p < 0.01, ***p < 0.001 compared with untreated group using one-way ANOVA with Turkey's Multiple Comparison Test.

## DISCUSSION

In this study we show that GELNs are selectively taken up by the oral pathogen *P. gingivalis*. This selectivity is determined by GELN-derived lipid PA, which interacts with hemin-binding protein 35 (HBP35) expressed on the surface of *P. gingivalis*. HBP35 is a functionally versatile protein involved in hemin uptake, colonization of epithelial surfaces, and biofilm development through binding to various oral Gram-positive and Gram-negative bacteria (Hiratsuka et al., 2010) (Hiratsuka et al., 2008). Our results showed that binding of HBP35 with GELN PA leads to inhibition of *P. gingivalis* growth. This conclusion is further supported by the finding that depletion of PA from GELNs or loss of HBP35 in *P. gingivalis* leads to no HBP35/PA interaction and consequently no disruption of *P. gingivalis* membrane. In addition, we found that pre-incubation of GELN with HBP35 peptide comprising the active binding domain prevents GELN-mediated inhibition of growth of *P. gingivalis*. At the molecular level, we further defined that the specificity of PA binding to HBP35 is dependent on the degree of unsaturation of PA. It has been shown that PA recruits and activates effector molecules that change the biophysical properties of the mammalian cell membrane and directly induce membrane destabilization (Athenstaedt and Daum, 1999; Kooijman et al., 2003). However, the effect of PA on the bacterial membrane has not been reported before. Collectively, these results suggest that GELN PA is required for selective uptake by *P. gingivalis* via interaction with the HBP35-binding domain. This finding is significant since the selectively of uptake could be exploited not only for targeting specific bacteria but also for delivery of therapeutic agents to specific pathogens for treatment.

Previous studies have shown that both secreted and surface-associated proteins contribute to the virulence of *P. gingivalis*. Arg-gingipain, Lys-gingipain, and hemagglutinins are among the major virulence factors of *P. gingivalis* (Savett and Progulske-Fox, 1995; Veith et al., 2002). In this study, we showed that GELN and its component lipids and miRNAs decreased significantly gingipain activities and hemagglutinin expression in *P. gingivalis*. Furthermore, we found that miR-159a-3p has several potential binding sites on the 3'-UTR of genes encoding gingipain and hemagglutinin. This finding provides a foundation for further study of the molecular mechanisms underlying plant exosome-like nanoparticle inhibition of oral bacterial pathogenicity via plant miRNA interaction with pathogenic factors such as gingipain and hemagglutinin. Furthermore, other GELN molecules can also participate in inhibition of bacterial pathogenicity. We identified GELN PA binding to the proteins containing the T9SS conserved C-terminal domain (CTD), including gingipain and hemagglutinin. The Type IX secretion system is composed of several outer membrane, periplasmic, and inner membrane proteins that play a role in gingipain secretion and transport other virulence factors to the host environment. Mutation of these proteins leads to accumulation of gingipain in the periplasm and non-pigmented colony morphology (de Diego et al., 2016; Lasica et al., 2016; Vincent et al., 2017). In the present study, we observed that GELN and its lipids and miRNAs decreased significantly the expression of T9SS in *P. gingivalis*. In addition to these virulence factors, GELNs, lipid, and miRNA also
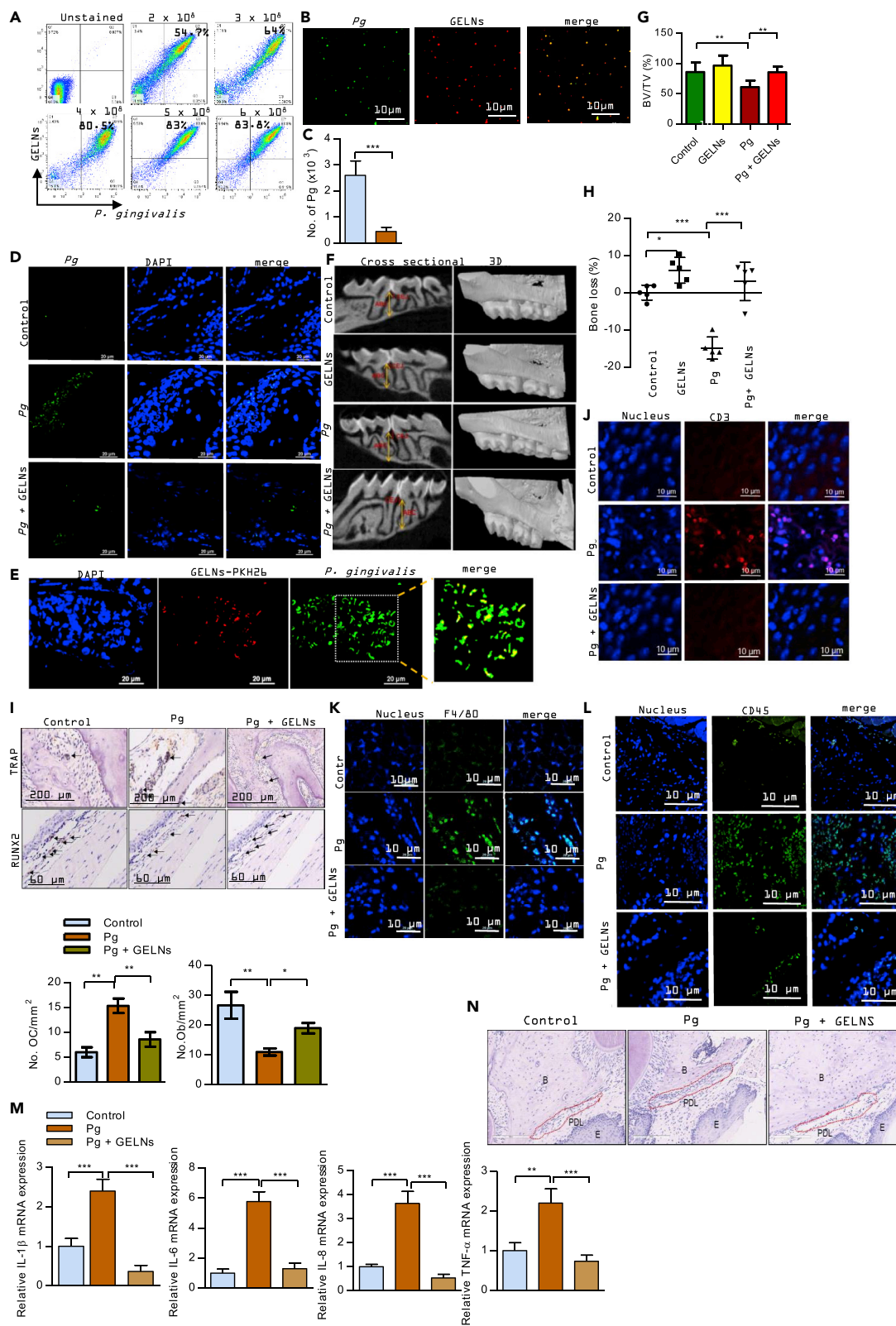
**Figure 8. Effect of GELNs on *P. gingivalis*-Induced Bone Loss *In Vivo***

(A) *P. gingivalis* and GELNs were fluorescently labeled with PKH67 and PKH26, respectively. *P. gingivalis* ($10^8$) was inoculated into the oral cavity, and GELNs ($6.0 \times 10^8$ particles) were applied to the oral cavity for 1 h. After washing, bacteria were collected with a sterile swab and uptake of GELNs was quantified by flow cytometry.

(B) *P. gingivalis* uptake of GELNs in the oral cavity was determined by confocal microscopy.

(C) *P. gingivalis* ($10^8$) was inoculated into the mouse oral cavity. The mice were given GELNs ($4.0 \times 10^8$ particles/mL) *ad libitum* in drinking water. Three weeks after the final inoculation, the numbers of *P. gingivalis* were determined by qPCR.

(D) The presence of *P. gingivalis* in the oral tissue was determined by confocal microscopy. Oral tissue sections were stained with anti-*P. gingivalis* antibody followed by fluorescent Alexa Fluor 488-labeled secondary antibody. The presence of *P. gingivalis* was visualized by confocal microscopy. The nucleus was stained with DAPI.

(E) *In vivo* GELNs taken up by *P. gingivalis* were determined by confocal microscopy. *P. gingivalis* was inoculated in the mouse oral cavity three times on alternative days. Then, PKH26 labeled GELNs were added into the drinking water for 24 h. GELNs taken up by *P. gingivalis* in oral tissue were stained with anti-*P. gingivalis* followed by fluorescent Alexa Fluor 488-labeled secondary antibody. The GELN taken up by *P. gingivalis* was visualized by confocal microscopy.

(F) Linear measurements were taken from the cementoenamel junction (CEJ) to the alveolar bone crest (ABC) in the interdental space to measure alveolar bone loss. Images on the left are representative of 14 cross sections measured across the maxillary molars. On the right, three-dimensional reconstructed renderings are shown for representative specimens in each group, such as control (uninfected), GELNs (control mice drank GELNs), Pg (*P. gingivalis* infected), and Pg + GELNs (*P. gingivalis* infected mice continuously drank GELNs). The *P. gingivalis*-treated group shows clear exposure of the tooth root that is not observed when treated with GELNs.

(G) Quantification of alveolar bone fraction from the micro-CT three-dimensional image of alveolar bone crest of region of interest (ROI).

(H) Alveolar bone loss was measured by the distance between the ABC and CEJ at 14 predetermined points on the maxillary molars sites. Each symbol represents an individual mouse, and the short horizontal lines indicates the mean.

(I–L) (I) TRAP staining of an oral tissue section to determine osteoclast (OC) number, and RUNX2 expression for osteoblasts (OB) in an oral tissue section was determined by immunohistochemistry. The number of TRAP-positive multinucleated OCs and RUNX2-positive OBs was counted manually. (J–L) Oral tissue sections were stained with anti-CD3, anti-F4/80, and anti-CD45 antibodies followed by fluorescent labeled secondary antibodies. The expression of CD3, F4/80, and CD45 was visualized by confocal microscopy.

(M) Total RNA was isolated from the control and experimental mice oral tissue and analyzed by RT-qPCR for expression of mRNA for inflammatory and bone resorptive cytokines IL-1β, IL-6, IL-8, and TNF-α. Results are expressed as mean ± standard deviation from three independent experiments.

(N) Hematoxylin staining of oral section of control, *P. gingivalis*-infected mice, and GELN-treated mice. B, alveolar bone crest; PDL, periodontal ligament; E, epithelial cells.

Results are expressed as mean ± standard deviation from three independent experiments. *p < 0.05, **p < 0.01, ***p < 0.001 compared with an untreated group using a one-way ANOVA with the Turkey's Multiple Comparison Test.

inhibited expression of other important *P. gingivalis* components such as OmpA, rod shape determining protein A (RodA), and the AraC transcriptional regulators. The AraC family of transcription regulators is one of the largest group of regulatory proteins in bacteria and can control the expression of several virulence factors in a variety of organisms (Yang et al., 2011). Collectively, our findings suggest that GELNs carry a broad spectrum of molecules, including lipids and miRNAs, that can inhibit multiple pathways in *P. gingivalis*.

Besides GELNs, the fact that all other types of edible plant exosome-like nanoparticles (ELNs) carry a broad spectrum of molecules supports further examination as to whether other ELNs have a role in inhibition of pathogenic factor(s) or/and promoting beneficial factor(s) from oral bacteria to regulating oral bacterial homeostasis. Over 700 bacterial species may be found in the oral cavity of humans (Paster et al., 2006). The diverse community that makes up the oral microbiome is of great importance in maintaining homeostasis. Oral dysbiosis contributes to the development of periodontitis. *P. gingivalis* is considered a keystone pathogen (Hajishengallis et al., 2012), and thus targeting of this organism may be sufficient to ameliorate or prevent disease. In this regard, in non-human primates where *P. gingivalis* is a natural inhabitant of the subgingival biofilm, immunization against *P. gingivalis* gingipain proteases causes a reduction in *P. gingivalis* numbers, total subgingival bacterial load, and bone loss (Page et al., 2007). Nonetheless, as periodontitis involves a community of organisms (Lamont et al., 2018), the ability of GELNs to modulate the pathogenic potential of other potential pathogens (e.g., *Tannerella forsythia*, *Prevotella intermedia*, *Aggregatibacter actinomycetemcomitans*, *Treponema denticola*, *Filifactor alocis*) alone and in the context of a heterotypic biofilm community also requires further study. The results presented in our previous report (Teng et al., 2018) imply that ginger edible exosome-like nanoparticles are taken up by a group of gut bacteria and have a role in maintaining gut microbiota homeostasis by inhibiting the growth of potential pathogens as well as increasing beneficial bacterial survival. The current study opens up a new avenue for studying whether a combination of other types of ELNs with GELNs can target more species than *P. gingivalis* to have greater potency in inhibiting the development of periodontitis. Collectively, this study further supports the hypothesis that edible plant exosome-like nanoparticles packaging various agents can

target multiple virulence factors of infectious agents simultaneously for the prevention/treatment of infectious diseases. Since pathogenicity in general is multifactorial, the action of edible plant exosome-like nanoparticles (ELNs) is likely to be more efficient than that of any single molecule. ELNs have the potential to be further developed as a new source of prebiotics. In addition, currently, only a subset of gut and oral bacteria can be grown in the laboratory in pure culture (Stewart, 2012), and systematic approaches to identifying growth conditions for as yet uncultivable bacteria have been challenging (Vartoukian et al., 2010). Our findings also suggest the possibility of *in vitro* co-culturing of oral or gut bacteria with ELNs for enhancing growth.

The interaction of bacterial factors with host cells contributes to *P. gingivalis* colonization and pathogenicity. Several *P. gingivalis* proteins, including the FimA component fimbriae (fimA) and the Mfa1 component fimbriae, play a role in attachment to host surfaces (Lin et al., 2006) (Hamada et al., 1996) (Zheng et al., 2011). Our study showed that GELNs and their component lipids and miRNAs significantly reduced FimA expression and further inhibited attachment of *P. gingivalis* to oral epithelial cells. We also showed that treatment with GELNs significantly diminished *P. gingivalis*-induced alveolar bone loss in a mouse model. Moreover, GELNs impacted the immune response and we observed a decrease in the expression of bone resorptive cytokines, including IL-1β, IL-6, Il-8, and TNF-α, and decreased recruitment of macrophages, leukocytes, and CD3 cells into the oral tissue microenvironment. The data published also indicate that GELNs also have anti-inflammatory properties. Whether this GELN-mediated immune modulation is through direct interaction of GELNs with CD3 T cells and macrophages or through metabolites released by GELN-responsive oral bacteria cannot be distinguished in the standard *in vivo* periodontal bone loss model utilized in this study, and the relative importance of GELN effects on bacteria or host immunity requires further investigation. Indeed, GELNs may provide a two-hit effect, i.e., antibacterial and anti-inflammatory. Interestingly, we also found that naive mice treated with GELNs in the drinking water have higher bone mineral density than control naive mice. This finding will open up a new avenue to study how GELNs can improve the bone mineral density in general since disruption of bone metabolism is associated with many diseases.

### Limitations of the Study

One limitation of this study is that we examined the effect of GELNs on *in vitro* monospecies biofilm formation, which is not representative of the influence of GELNs on established polymicrobial biofilms. Therefore, further studies are needed to determine if GELNs can penetrate an established microbial biofilm and have an influence of polymicrobial interactions and on the antibiotic susceptibility of biofilms. Additionally, the impact of GELNs on pre-existing multispecies biofilms, such as those that occur in human *in vivo*, requires further study.

### METHODS

All methods can be found in the accompanying Transparent Methods supplemental file.

### SUPPLEMENTAL INFORMATION

Supplemental Information can be found online at https://doi.org/10.1016/j.isci.2019.10.032.

### AUTHOR CONTRIBUTIONS

K.S., D.P.M., X.Z., Y.T., R.J.L., and H.-G.Z. designed the study, analyzed, interpreted data, and prepared the manuscript; K.S. and D.P.M. performed experiments and interpreted data; J.W.P. and M.S. provided bioinformatics analysis and quantitation; C.L., L.H., and Y.F. provided HPLC analysis; J.M. provided histological analysis; A.K., M.K.S., C.L., and K.S. prepared GELNs and bacteria; M.L.M. did protein analysis; L.Z. provided technical support; S.Q.Z, Y.J., and X.Z interpreted the findings.

## REFERENCES

Alvarez-Erviti, L., Seow, Y., Yin, H., Betts, C., Lakhal, S., and Wood, M.J. (2011). Delivery of siRNA to the mouse brain by systemic injection of targeted exosomes. Nat. Biotechnol. *29*, 341–345.

Athenstaedt, K., and Daum, G. (1999). Phosphatidic acid, a key intermediate in lipid metabolism. Eur. J. Biochem. *266*, 1–16.

Baker, P.J., Dixon, M., Evans, R.T., Dufour, L., Johnson, E., and Roopenian, D.C. (1999). CD4(+) T cells and the proinflammatory cytokines gamma interferon and interleukin-6 contribute to alveolar bone loss in mice. Infect. Immun. *67*, 2804–2809.

Baker, P.J., Dixon, M., and Roopenian, D.C. (2000). Genetic control of susceptibility to *Porphyromonas gingivalis*-induced alveolar bone loss in mice. Infect. Immun. *68*, 5864–5868.

Bao, K., Belibasakis, G.N., Thurnheer, T., Aduse-Opoku, J., Curtis, M.A., and Bostanci, N. (2014). Role of *Porphyromonas gingivalis* gingipains in multi-species biofilm formation. BMC Microbiol. *14*, 258.

Baron, C. (2013). A novel strategy to target bacterial virulence. Future Microbiol. *8*, 1–3.

de Diego, I., Ksiazek, M., Mizgalska, D., Koneru, L., Golik, P., Szmigielski, B., Nowak, M., Nowakowska, Z., Potempa, B., Houston, J.A., et al. (2016). The outer-membrane export signal of *Porphyromonas gingivalis* type IX secretion system (T9SS) is a conserved C-terminal beta-sandwich domain. Sci. Rep. *6*, 23123.

Goldberg, K., Sarig, H., Zaknoon, F., Epand, R.F., Epand, R.M., and Mor, A. (2013). Sensitization of gram-negative bacteria by targeting the membrane potential. FASEB J. *27*, 3818–3826.

Hajishengallis, G., Darveau, R.P., and Curtis, M.A. (2012). The keystone-pathogen hypothesis. Nat. Rev. Microbiol. *10*, 717–725.

Hamada, N., Sojar, H.T., Cho, M.I., and Genco, R.J. (1996). Isolation and characterization of a minor fimbria from *Porphyromonas gingivalis*. Infect. Immun. *64*, 4788–4794.

Hiratsuka, K., Hayakawa, M., Kiyama-Kishikawa, M., Sasaki, Y., Hirai, T., and Abiko, Y. (2008). Role of the hemin-binding protein 35 (HBP35) of *Porphyromonas gingivalis* in coaggregation. Microb. Pathog. *44*, 320–328.

Hiratsuka, K., Kiyama-Kishikawa, M., and Abiko, Y. (2010). Hemin-binding protein 35 (HBP35) plays an important role in bacteria-mammalian cells interactions in *Porphyromonas gingivalis*. Microb. Pathog. *48*, 116–123.

Kauppi, A.M., Nordfelth, R., Uvell, H., Wolf-Watz, H., and Elofsson, M. (2003). Targeting bacterial virulence: inhibitors of type III secretion in Yersinia. Chem. Biol. *10*, 241–249.

Kooijman, E.E., Chupin, V., de Kruijff, B., and Burger, K.N. (2003). Modulation of membrane curvature by phosphatidic acid and lysophosphatidic acid. Traffic *4*, 162–174.

Lam, R.S., O'Brien-Simpson, N.M., Lenzo, J.C., Holden, J.A., Brammar, G.C., Walsh, K.A., McNaughtan, J.E., Rowler, D.K., Van Rooijen, N., and Reynolds, E.C. (2014). Macrophage depletion abates *Porphyromonas gingivalis*-induced alveolar bone resorption in mice. J. Immunol. *193*, 2349–2362.

Lamont, R.J., Chan, A., Belton, C.M., Izutsu, K.T., Vasel, D., and Weinberg, A. (1995). *Porphyromonas gingivalis* invasion of gingival epithelial cells. Infect. Immun. *63*, 3878–3885.

Lamont, R.J., Koo, H., and Hajishengallis, G. (2018). The oral microbiota: dynamic communities and host interactions. Nat. Rev. Microbiol. *16*, 745–759.

Lasica, A.M., Goulas, T., Mizgalska, D., Zhou, X., de Diego, I., Ksiazek, M., Madej, M., Guo, Y., Guevara, T., Nowak, M., et al. (2016). Structural and functional probing of PorZ, an essential bacterial surface component of the type-IX secretion system of human oral-microbiomic *Porphyromonas gingivalis*. Sci. Rep. *6*, 37708.

Lasica, A.M., Ksiazek, M., Madej, M., and Potempa, J. (2017). The type IX secretion system (T9SS): highlights and recent insights into its structure and function. Front. Cell. Infect. Microbiol. *7*, 215.

Lin, X., Wu, J., and Xie, H. (2006). *Porphyromonas gingivalis* minor fimbriae are required for cell-cell interactions. Infect. Immun. *74*, 6011–6015.

Liu, L.S., Gkranias, N., Farias, B., Spratt, D., and Donos, N. (2018). Differences in the subgingival microbial population of chronic periodontitis in subjects with and without type 2 diabetes mellitus-a systematic review. Clin. Oral Invest. *22*, 2743–2762.

Miki, T., and Hardt, W.D. (2013). Outer membrane permeabilization is an essential step in the killing of gram-negative bacteria by the lectin RegIIIbeta. PLoS One *8*, e69901.

Mu, J., Zhuang, X., Wang, Q., Jiang, H., Deng, Z.B., Wang, B., Zhang, L., Kakar, S., Jun, Y., Miller, D., et al. (2014). Interspecies communication between plant and mouse gut host cells through edible plant derived exosome-like nanoparticles. Mol. Nutr. Food Res. *58*, 1561–1573.

Nusslein, K., Arnt, L., Rennie, J., Owens, C., and Tew, G.N. (2006). Broad-spectrum antibacterial activity by a novel abiogenic peptide mimic. Microbiology *152*, 1913–1918.

Olsen, I., Lambris, J.D., and Hajishengallis, G. (2017). *Porphyromonas gingivalis* disturbs host-commensal homeostasis by changing complement function. J. Oral Microbiol. *9*, 1340085.

Page, R.C., Lantz, M.S., Darveau, R., Jeffcoat, M., Mancl, L., Houston, L., Braham, P., and Persson, G.R. (2007). Immunization of *Macaca fascicularis* against experimental periodontitis using a vaccine containing cysteine proteases purified from *Porphyromonas gingivalis*. Oral Microbiol. Immunol. *22*, 162–168.

Pan, X., Yang, Y., and Zhang, J.R. (2014). Molecular basis of host specificity in human pathogenic bacteria. Emerg. Microbes Infect. *3*, e23.

Paster, B.J., Olsen, I., Aas, J.A., and Dewhirst, F.E. (2006). The breadth of bacterial diversity in the human periodontal pocket and other oral sites. Periodontol. 2000 *42*, 80–87.

Potempa, J., Sroka, A., Imamura, T., and Travis, J. (2003). Gingipains, the major cysteine proteinases and virulence factors of *Porphyromonas gingivalis*: structure, function and assembly of multidomain protein complexes. Curr. Protein Pept. Sci. *4*, 397–407.

Reyes, L., Phillips, P., Wolfe, B., Golos, T.G., Walkenhorst, M., Progulske-Fox, A., and Brown, M. (2018). *Porphyromonas gingivalis* and adverse pregnancy outcome. J. Oral Microbiol. *10*, 1374153.

Savett, D.A., and Progulske-Fox, A. (1995). Restriction fragment length polymorphism analysis of two hemagglutinin loci, serotyping and agglutinating activity of *Porphyromonas gingivalis* isolates. Oral Microbiol. Immunol. *10*, 1–7.

Shibata, Y., Okano, S., Shiroza, T., Tahara, T., Nakazawa, K., Kataoka, S., Ishida, I., Kobayashi, T., Yoshie, H., and Abiko, Y. (2011). Characterization of human-type monoclonal antibodies against reduced form of hemin binding protein 35 from *Porphyromonas gingivalis*. J. Periodontal Res. *46*, 673–681.

Shoji, M., Shibata, Y., Shiroza, T., Yukitake, H., Peng, B., Chen, Y.Y., Sato, K., Naito, M., Abiko, Y., Reynolds, E.C., et al. (2010). Characterization of

hemin-binding protein 35 (HBP35) in *Porphyromonas gingivalis*: its cellular distribution, thioredoxin activity and role in heme utilization. BMC Microbiol. *10*, 152.

Smalley, J.W., and Olczak, T. (2017). Heme acquisition mechanisms of *Porphyromonas gingivalis* - strategies used in a polymicrobial community in a heme-limited host environment. Mol. Oral Microbiol. *32*, 1–23.

Stewart, E.J. (2012). Growing unculturable bacteria. J. Bacteriol. *194*, 4151–4160.

Teng, Y., Ren, Y., Sayed, M., Hu, X., Lei, C., Kumar, A., Hutchins, E., Mu, J., Deng, Z., Luo, C., et al. (2018). Plant-derived exosomal MicroRNAs shape the gut microbiota. Cell Host Microbe *24*, 637–652.e8.

Tribble, G.D., and Lamont, R.J. (2010). Bacterial invasion of epithelial cells and spreading in periodontal tissue. Periodontol. 2000 *52*, 68–83.

Tzach-Nahman, R., Mizraji, G., Shapira, L., Nussbaum, G., and Wilensky, A. (2017). Oral infection with *Porphyromonas gingivalis* induces peri-implantitis in a murine model: evaluation of bone loss and the local inflammatory response. J. Clin. Periodontol. *44*, 739–748.

Vartoukian, S.R., Palmer, R.M., and Wade, W.G. (2010). Strategies for culture of 'unculturable' bacteria. FEMS Microbiol. Lett. *309*, 1–7.

Veith, P.D., Talbo, G.H., Slakeski, N., Dashper, S.G., Moore, C., Paolini, R.A., and Reynolds, E.C. (2002). Major outer membrane proteins and proteolytic processing of RgpA and Kgp of *Porphyromonas gingivalis* W50. Biochem. J. *363*, 105–115.

Vincent, M.S., Canestrari, M.J., Leone, P., Stathopulos, J., Ize, B., Zoued, A., Cambillau, C., Kellenberger, C., Roussel, A., and Cascales, E. (2017). Characterization of the *Porphyromonas gingivalis* Type IX secretion trans-envelope PorKLMNP core complex. J. Biol. Chem. *292*, 3252–3261.

Wang, Q., Zhuang, X., Mu, J., Deng, Z.B., Jiang, H., Zhang, L., Xiang, X., Wang, B., Yan, J., Miller, D., et al. (2013). Delivery of therapeutic agents by nanoparticles made of grapefruit-derived lipids. Nat. Commun. *4*, 1867.

Xiao, J., Feng, S., Wang, X., Long, K., Luo, Y., Wang, Y., Ma, J., Tang, Q., Jin, L., Li, X., et al. (2018). Identification of exosome-like nanoparticle-derived microRNAs from 11 edible fruits and vegetables. PeerJ *6*, e5186.

Yang, J., Tauschek, M., and Robins-Browne, R.M. (2011). Control of bacterial virulence by AraC-like

regulators that respond to chemical signals. Trends Microbiol. *19*, 128–135.

Zenobia, C., and Hajishengallis, G. (2015). *Porphyromonas gingivalis* virulence factors involved in subversion of leukocytes and microbial dysbiosis. Virulence *6*, 236–243.

Zheng, C., Wu, J., and Xie, H. (2011). Differential expression and adherence of *Porphyromonas gingivalis* FimA genotypes. Mol. Oral Microbiol. *26*, 388–395.

Zhuang, X., Deng, Z.B., Mu, J., Zhang, L., Yan, J., Miller, D., Feng, W., McClain, C.J., and Zhang, H.G. (2015). Ginger-derived nanoparticles protect against alcohol-induced liver damage. J. Extracell. Vesicles *4*, 28713.

Zhuang, X., Xiang, X., Grizzle, W., Sun, D., Zhang, S., Axtell, R.C., Ju, S., Mu, J., Zhang, L., Steinman, L., et al. (2011). Treatment of brain inflammatory diseases by delivering exosome encapsulated anti-inflammatory drugs from the nasal region to the brain. Molecular therapy. J. Am. Soc. Gene Ther. *19*, 1769–1779.

Zhuang, Z., Yoshizawa-Smith, S., Glowacki, A., Maltos, K., Pacheco, C., Shehabeldin, M., Mulkeen, M., Myers, N., Chong, R., Verdelis, K., et al. (2018). Induction of M2 macrophages prevents bone loss in murine periodontitis models. J. Dental Res. *98*, 200–208.

# Supplemental Information

# Plant-Derived Exosomal

# Nanoparticles Inhibit Pathogenicity

# of *Porphyromonas gingivalis*

Kumaran Sundaram, Daniel P. Miller, Anil Kumar, Yun Teng, Mohammed Sayed, Jingyao Mu, Chao Lei, Mukesh K. Sriwastva, Lifeng Zhang, Yan Jun, Michael L. Merchant, Liqing He, Yuan Fang, Shuangqin Zhang, Xiang Zhang, Juw W. Park, Richard J. Lamont, and Huang-Ge Zhang

# Supplemental Information

# Plant-Derived Exosomal Nanoparticles Inhibit Pathogenicity of *Porphyromonas gingivalis*

**Kumaran Sundaram, Daniel P. Mille, Anil Kumar , Yun Teng, Mohammed Sayed, Jingyao Mu, Chao Lei, Mukesh K Sriwastva, Lifeng Zhang, Yan Jun, Michael L Merchant, Liqing He, Yuan Fang, Shuang Qin Zhang, Xiang Zhang, Juw Won Park,  Richard J. Lamont, and Huang-Ge Zhang**

**Figure S1.  GELNs did not affect the growth of *S. gordonii*, Related to Figure 1.**
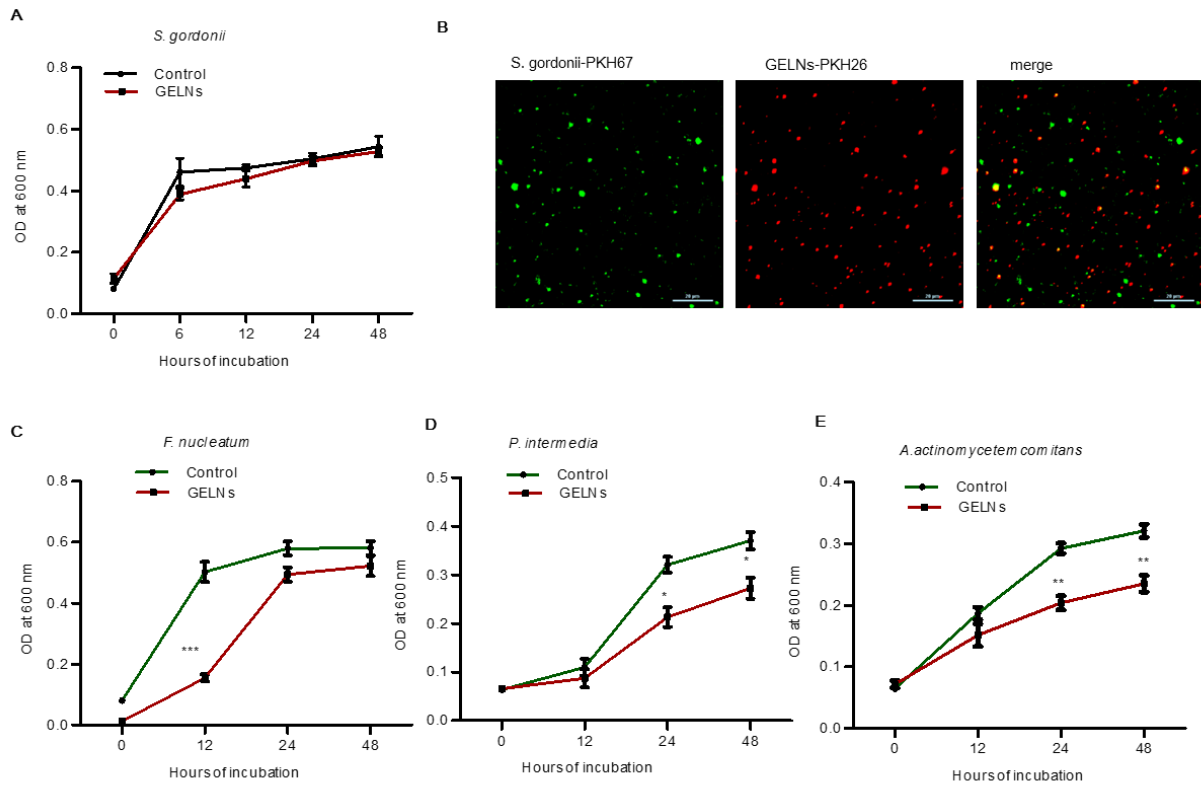


**(A)** *S. gordonii* was treated with GELNs (4.0 x10$^8$/ml) for the indicated times. **(B)** *S. gordonii* did not take up GELNs. *S. gordonii* and GELNs were labelled with fluorescent dyes PKH67 and PKH26, respectively. *S. gordonii* was incubated with GELNs for 1 h at 37°C. Uptake of GELNs by *S. gordonii* was determined using confocal microscopy. **(C-E)**. *F. nucleatum, P. intermedia and A. actinomycetemcomitans* was treated with GELNs (4.0 x10$^8$/ml) for the indicated times. The growth of *S. gordonii* was determined by measuring optical density at 600 nm. Results are expressed as mean ± standard deviation from three independent experiments. *P <0.05, **P<0.01, ***P<0.001 compared with an untreated group using a one-way ANOVA with the Turkey's Multiple Comparison Test.

**Figure S2. GELNs modulate inner membrane depolarization and membrane fluidity in
*P. gingivalis*, Related to Figure 1.**
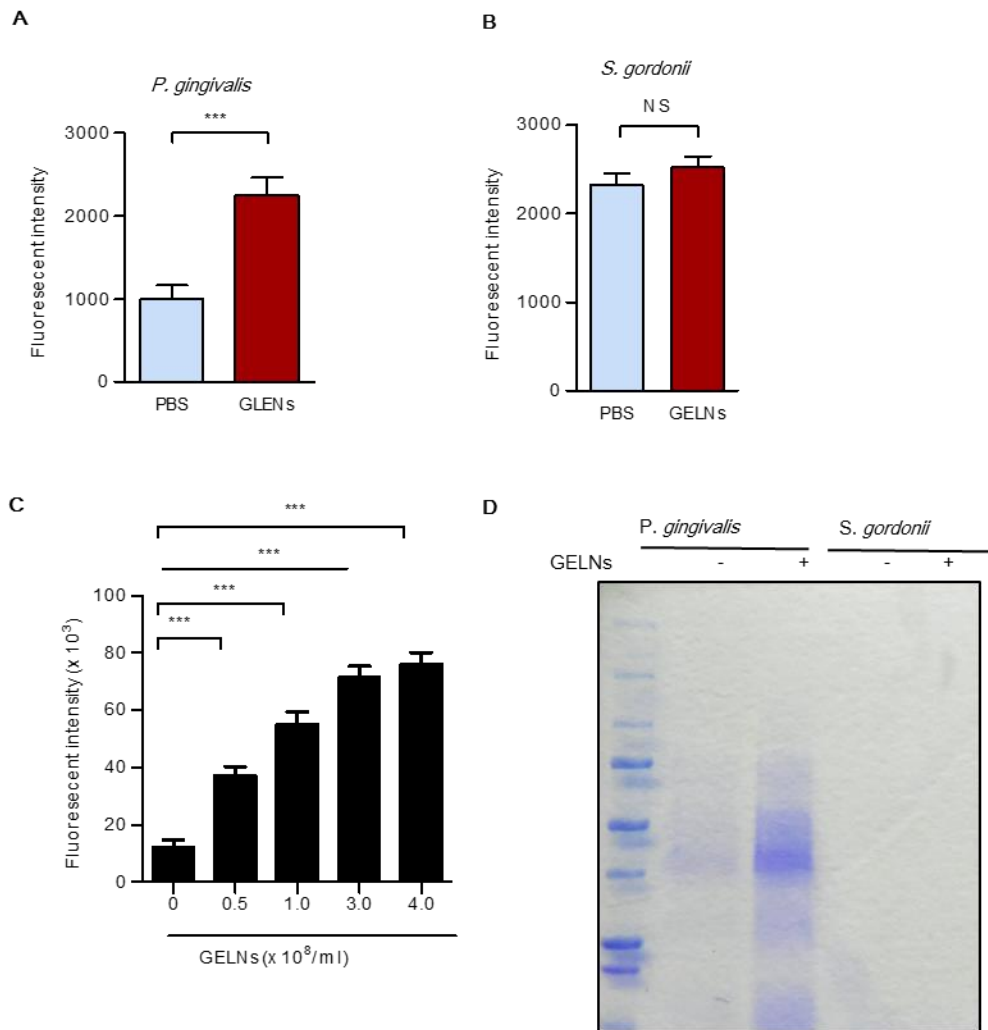


(A-B) *P. gingivalis* and *S. gordonii* were washed with HEPES–glucose buffer and incubated with 0.4 $\mu$M of diSC3-5 for 1 h.  Bacteria were treated with GELNs (6.0 x $10^8$ particles /ml) for 2 h. Membrane depolarization was measured by fluorescence intensity at 620 nm excitation and 722 nm emission. **(C)** *P. gingivalis* was incubated with different concentrations (0-6.0 x $10^8$ particles /ml) of GELNs for 2 h at 37°C and 0.5 $\mu$M of ethidium bromide was added. The fluorescent intensity was measured at 540 nm and 610 nm of excitation and emission, respectively. **(D)** *P. gingivalis* and *S. gordonii* were treated with GELNs (4.0 x $10^8$ particles /ml) for 24 h and centrifuged (10,000 rpm) for 10 min to remove bacteria. The supernatant was separated by SDS-PAGE and stained with Coomassie brilliant blue. Results are expressed as means ± standard deviation from three independent experiments. NS; Not significant, ***P<0.001 compared with an untreated control group using Student 't' Test.

**Figure S3. GELNs modulate metabolic pathways in *P. gingivalis*, Related to Figure 1.**

A



B
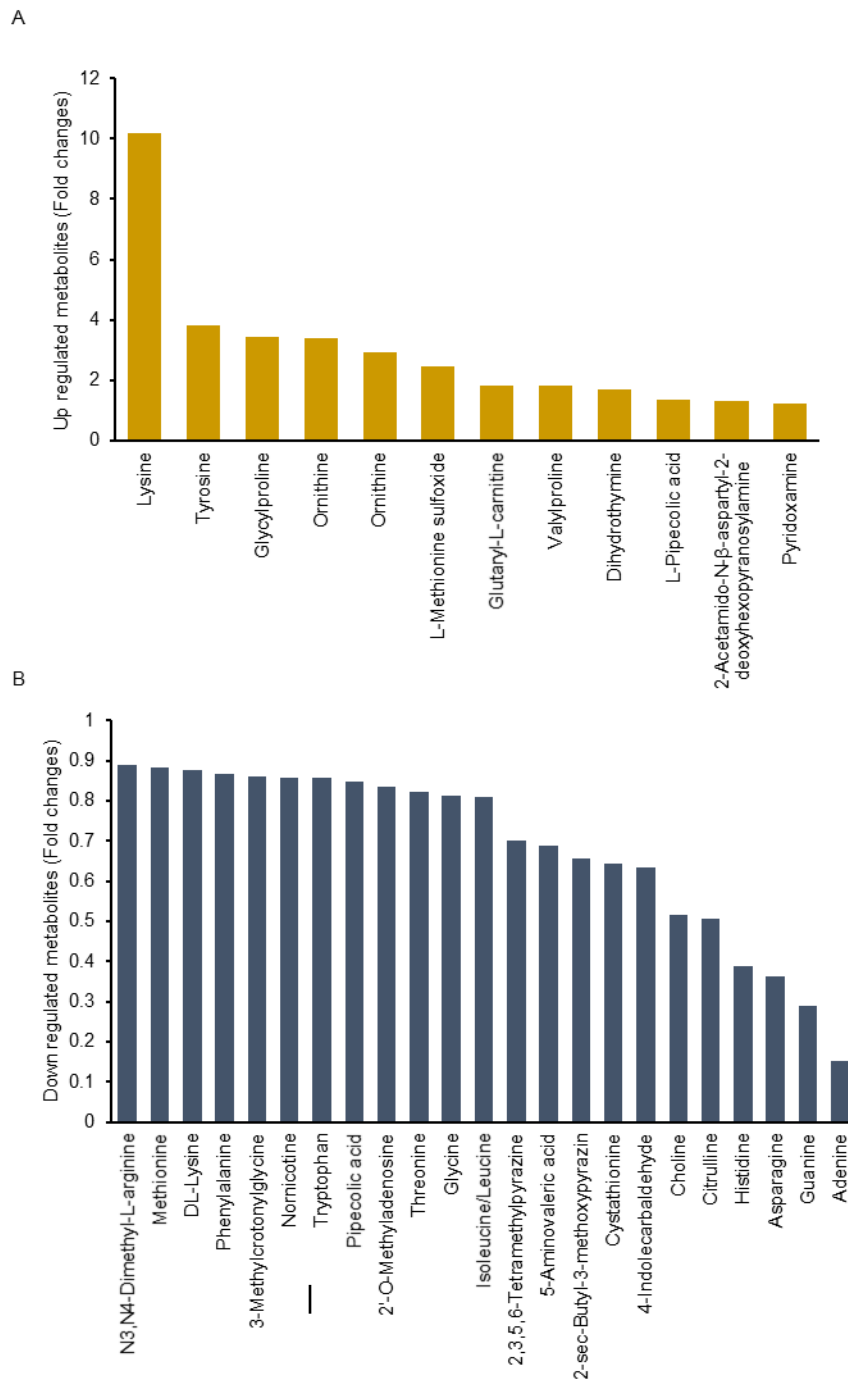


*P. gingivalis* was treated with GELNs (4 × 10$^8$ particles /ml) for 24 h. Metabolic product in the supernatant were measured by LC- MS. **(A)** upregulated metabolic products. **(B)** down regulated metabolic products.

**Table S1: Metabolies released by *P. gingivalis* released metabolites and their function, Related to Figure 1.**

| Metabolites | Function | Reference |
|---|---|---|
| Lysine | lysine, is required in protein synthesis and in the peptidoglycan layer of Gram-positive bacterial cell walls | (Gillner et al., 2013) |
| Tyrosine | D-tyrosine has potent activity toward biofilm disassembly | (Kolodkin-Gal et al., 2010) |
| Proline | Protection against abiotic stress, osmoregulation, protein stability, involved in cell signaling and energy production | (Christgen and Becker, 2018) |
| Ornithine | contribute to cytosolic pH homeostasis when cells are exposed to acidic environments | (Viala et al., 2011) |
| L- methionine sulfoxide | Defends against oxidative stress | (Luo and Levine, 2009) |
| L-Carnitine | Role in electron transport chain, osmoprotection, served as nutrient | (Meadows and Wargo, 2015) |
| L-pipecolic acid | served as carbon and nitrogen source | (Rao and Rodwell, 1962) |
| Pyridoxamine | Serves as cofactor of enzymes, role in amino acid and fatty acid metabolism | (El Qaidi et al., 2013) |
| Dimethyl -L-arginine | Involved in several metabolic pathway and role in bacterial pathogenesis | (Xiong et al., 2016) |
| Methionine | Initiation of translation, it is common cofactor | (Ferla and Patrick, 2014) |
| Phenylalanine | Degradation by several anaerobic bacteria and important for growth | (Fuchs et al., 2011) |
| 3-Methylcrotonglycine | Modulates mitochondrial energy production and inhibit ATPase | (Moura et al., 2012) |
| 2'-Methyladenosine | Involved in gene regulation | (Deng et al., 2015) |
| Threonine | Phosphorylation of protein which play an important role in pathogenesis, host cell interaction | (Cozzone, 2005) |
| Glycine | Inhibit bacterial growth, inhibit synthesis peptidoglycan on bacterial cell wall | (Hammes et al., 1973) |
| Isoleucine | Role in bacterial growth | (Conner and Hansen, 1967) |
| Tetramethylpyrazine | Bacteria used for carbon and energy source | (Kutanovas et al., 2013) |
| 5-Aminovaleric acid | Bacterial catabolic product of Lysine and play a role in biotransformation | (Liu et al., 2014) |
| Cystathionine | Metabolites used for methionine biosynthesis | (Delavier-Klutchko and Flavin, 1965) |
| 4-Indoleccarbaldehyde | Biofilm formation, virulence factor production, antibiotic resistance. | (Melander et al., 2014) |
| Choline | It is precursor to GB, and GB act as a potent osmoprotectant and roles in shaping microbial communities | (Wargo, 2013) |
| Citruline | Protects bacteria from acid stress | (Cusumano and Caparon, 2015) |
| Histidine | Used as a source of carbon, energy, and nitrogen | (Bender, 2012) |
| Asparagine | Important role in glycoprotein biosynthesis | (Hart, 1982) |
| Guanine | Bacterial genomic DNA | (Muto and Osawa, 1987) |
| Adenine | Adenine Methylation play a role in Regulating Bacterial Gene Expression and Virulence | |

**Figure S4. miRNA profile of GELNs, Related to Figure 2.**
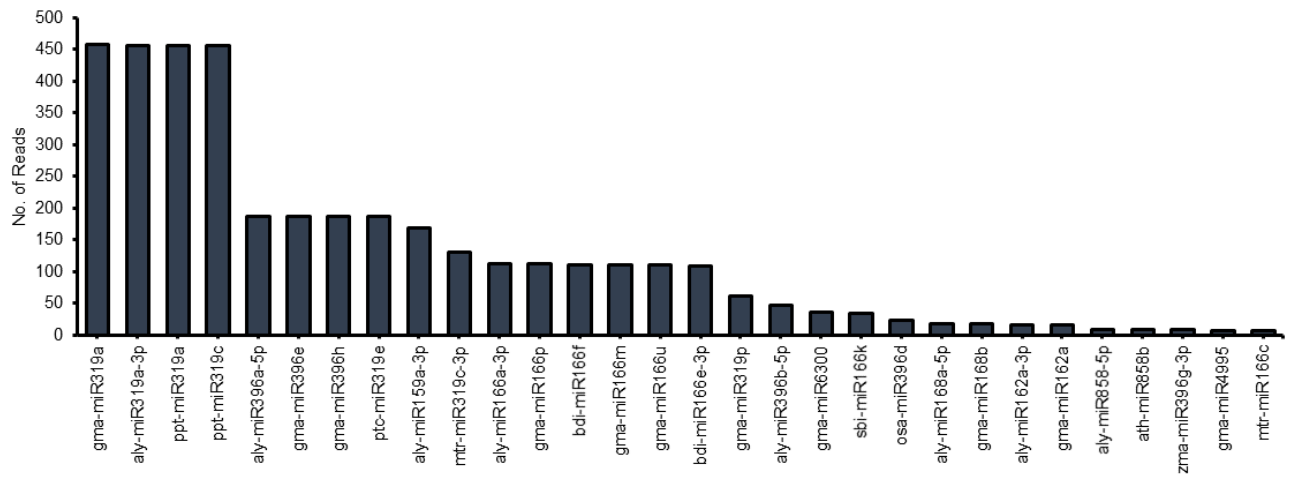


Total miRNA was extracted from the GELNs and the miRNA profile was determined as described in the Materials and Methods.

**Table S2: GELN-derived miRNA targeting *P. gingivalis* gene, Related to Figure 2.**

**Aly-miR-159a-3p**

| miRNA_seed | Gene symbol | locus_tag | Description |
|---|---|---|---|
| TTTGGATT | PGN_RS08230 | PGN_1733 | hemagglutinin |
| TTTGGATT | PGN_RS05900 | PGN_1227 | hypothetical protein |
| TTTGGATT | PGN_RS06005 | PGN_1253 | hypothetical protein |
| TTTGGATT | PGN_RS05790 | PGN_1204 | aspartate 1-decarboxylase |
| TTTGGATT | PGN_RS04300 | PGN_0902 | anaphase-promoting protein subunit 3 |
| TTTGGATT | PGN_RS05310 | | hypothetical protein |
| TTTGGATT | PGN_RS08315 | PGN_1750 | 3-deoxy-manno-octulosonate cytidylyltransferase |
| TTTGGATT | PGN_RS02060 | PGN_0433 | phosphoglycerate kinase |
| TTTGGATT | PGN_RS03450 | PGN_0723 | succinate-semialdehyde dehydrogenase |
| TTTGGATT | PGN_RS01525 | PGN_0318 | precorrin-3B C(17)-methyltransferase |
| TTTGGATT | PGN_RS04735 | PGN_0988 | hypothetical protein |
| TTTGGATT | PGN_RS07385 | PGN_1549 | ATP-dependent Clp protease proteolytic subunit |
| TTTGGATT | PGN_RS03750 | PGN_0786 | hypothetical protein |
| TTTGGATT | PGN_RS06440 | PGN_1349 | S9 family peptidase |
| TTTGGATT | PGN_RS09345 | PGN_1976 | hypothetical protein |
| TTTGGATT | PGN_RS02890 | PGN_0606 | glucosamine-6-phosphate deaminase |
| TTTGGATT | PGN_RS03215 | PGN_0675 | thiazole biosynthesis protein ThiJ |
| TTTGGATT | PGN_RS04470 | PGN_0935 | hypothetical protein |
| TTTGGATT | PGN_RS07600 | PGN_1594 | DNA topoisomerase IV subunit B |
| TTTGGATT | PGN_RS03485 | PGN_0732 | hypothetical protein |
| TTTGGATT | PGN_RS08125 | PGN_1708 | magnesium chelatase |
| TTTGGATT | PGN_RS00715 | PGN_0152 | T9SS C-terminal target domain-containing protein |
| TTTGGATT | PGN_RS00200 | PGN_0043 | cell division protein FtsH |
| TTTGGATT | PGN_RS00390 | PGN_0082 | AraC family transcriptional regulator |
| TTTGGATT | PGN_RS06580 | PGN_1381 | alanine--tRNA ligase |
| TTTGGATT | PGN_RS00600 | PGN_0128 | hypothetical protein |
| TTTGGATT | PGN_RS05340 | PGN_1115 | hemagglutinin |
| TTTGGATT | PGN_RS00370 | PGN_0079 | hypothetical protein |
| TTTGGATT | PGN_RS04995 | PGN_1042 | cytochrome D ubiquinol oxidase subunit II |
| TTTGGATT | PGN_RS02750 | | mobilization protein |
| TTTGGATT | PGN_RS05560 | PGN_1159 | anaphase-promoting protein subunit 3 |
| TTTGGATT | PGN_RS09285 | PGN_1963 | hypothetical protein |
| TTTGGATT | PGN_RS00415 | PGN_0087 | hypothetical protein |
| TTTGGATT | PGN_RS01490 | PGN_0311 | DUF4271 domain-containing protein |
| TTTGGATT | PGN_RS04225 | PGN_0884 | organic solvent tolerance protein OstA |
| TTTGGATT | PGN_RS09490 | PGN_2005 | hypothetical protein |
| TTTGGATT | PGN_RS00890 | PGN_0192 | membrane protein |
| TTTGGATT | PGN_RS09325 | PGN_1970 | peptidase C25 |
| TTTGGATT | PGN_RS09955 | PGN_1340 | hypothetical protein |
| TTTGGATT | PGN_RS01395 | PGN_0291 | VWA domain-containing protein |

**gma-miR166u**

| miRNA_seed | Gene symbol | locus_tag | Description |
|---|---|---|---|
| TCTCGGAC | PGN_RS04795 | PGN_1001 | DNA polymerase III subunit delta |
| TCTCGGAC | PGN_RS00800 | PGN_0172 | hypothetical protein |
| TCTCGGAC | PGN_RS05480 | PGN_1143 | hypothetical protein |
| TCTCGGAC | PGN_RS05135 | PGN_1070 | radical SAM protein |
| TCTCGGAC | PGN_RS06355 | PGN_1330 | branched-chain amino acid ABC transporter ATP-binding protein |
| TCTCGGAC | PGN_RS07035 | PGN_1475 | 5'-methylthioadenosine/S-adenosylhomocysteine nucleosidase |
| TCTCGGAC | PGN_RS05385 | PGN_1124 | paraslipin |
| TCTCGGAC | PGN_RS06240 | PGN_1305 | N-acetylmuramoyl-L-alanine amidase |
| TCTCGGAC | PGN_RS09395 | PGN_1986 | histidinol phosphate phosphatase |
| TCTCGGAC | PGN_RS07020 | PGN_1471 | membrane protein |
| TCTCGGAC | PGN_RS03965 | PGN_0831 | transcription antitermination factor NusB |
| TCTCGGAC | PGN_RS00960 | PGN_0205 | AraC family transcriptional regulator |
| TCTCGGAC | PGN_RS08890 | PGN_1874 | 3-phosphoshikimate 1-carboxyvinyltransferase |
| TCTCGGAC | PGN_RS00680 | PGN_0144 | DUF5103 domain-containing protein |
| TCTCGGAC | PGN_RS02140 | PGN_0446 | ABC transporter ATP-binding protein |
| TCTCGGAC | PGN_RS03390 | PGN_0710 | indolepyruvate ferredoxin oxidoreductase |
| TCTCGGAC | PGN_RS05550 | PGN_1157 | lysine--tRNA ligase |
| TCTCGGAC | PGN_RS04840 | PGN_1011 | adenine permease |
| TCTCGGAC | PGN_RS00735 | PGN_0157 | 2-iminoacetate synthase ThiH |
| TCTCGGAC | PGN_RS00090 | PGN_0017 | sodium-independent anion transporter |
| TCTCGGAC | PGN_RS03905 | PGN_0817 | penicillin-binding protein 1A |
| TCTCGGAC | PGN_RS09895 | PGN_2083 | potassium transporter |
| TCTCGGAC | PGN_RS00980 | PGN_0209 | glycine--tRNA ligase |
| TCTCGGAC | PGN_RS01460 | PGN_0303 | peptidase M16 |
| TCTCGGAC | PGN_RS09845 | PGN_2075 | excinuclease ABC subunit A |
| TCTCGGAC | PGN_RS02640 | PGN_0556 | cobaltochelatase |
| TCTCGGAC | PGN_RS09725 | PGN_2050 | helicase UvrD |

**gma-miR166p**

| miRNA_seed | Gene symbol | locus_tag | Description |
|---|---|---|---|
| TCGGACCA | PGN_RS01275 | PGN_0264 | signal recognition particle-docking protein FtsY |
| TCGGACCA | PGN_RS01430 | PGN_0299 | outer membrane protein assembly factor |
| TCGGACCA | PGN_RS03345 | PGN_0701 | beta-galactosidase |

**Figure S5. miRNA from GELNs did not affect the growth of *P.gingivalis*, Related to Figure 2.**
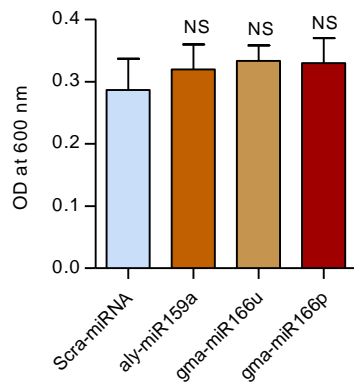


miRNAs aly-miR-159a, gma-miR166u or gma-miR-166p were packaged into lipid nanoparticles and incubated with *P. gingivalis* for 24 h. The growth of *P. gingivalis* was determined by measuring the optical density at 600 nm. Results are expressed as mean ± standard deviation from three independent experiments. NS; not significant compared with an scrambled miRNA transduced group using Student 't' Test.

**Figure S6. miRNA and lipids from GLENs have independent roles in *P. gingivalis* growth, Related to Figure 2.**
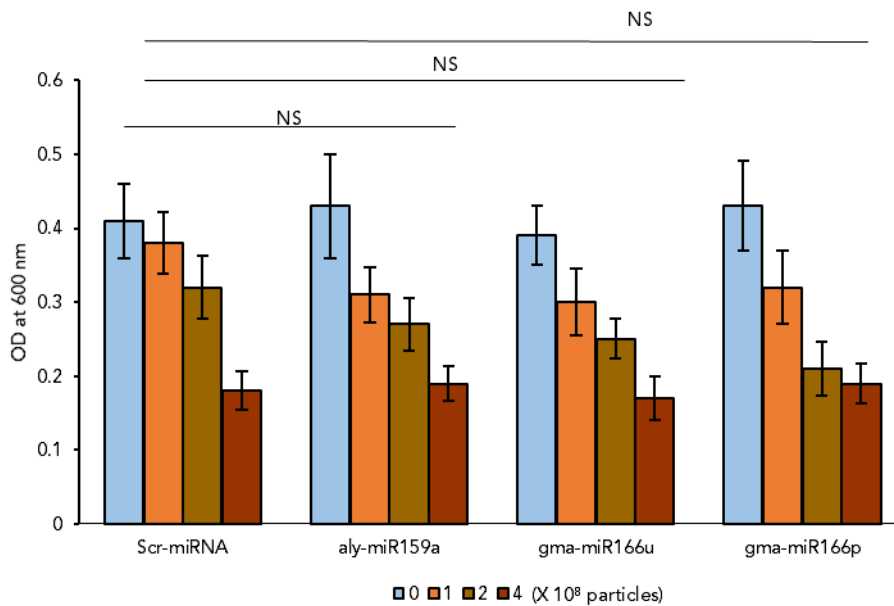


*P. gingivalis* was transduced with scrambled miRNA, aly-miR159a, gma-miR166u or gma-miR166p or treated with total lipids extracted from different concentrations of GELNs (0- $4.0 \times 10^8$ particles) and incubated for 24 h. The growth of *P. gingivalis* was measured by optical density at 600 nm. Results are expressed as means with standard deviation from three independent experiments. NS; Not significant represents the comparison of each miRNA with Scr-miRNA with lipid treatment by two-way ANOVA.

**Table S3: Lipid profile of GELNs, Related to Figure 2.**

| Mass | Compound Formula | Compound Name | nmol per mg dry wt |
|---|---|---|---|
| DGDG | | | |
| 958.6 | C51H88O15 | DGDG(36:4) | 138.65 |
| 960.6 | C51H90O15 | DGDG(36:3) | 119.80 |
| 936.6 | C49H90O15 | DGDG(34:1) | 97.43 |
| 962.6 | C51H92O15 | DGDG(36:2) | 57.25 |
| 934.6 | C49H88O15 | DGDG(34:2) | 42.90 |
| 956.6 | C51H86O15 | DGDG(36:5) | 29.63 |
| 964.7 | C51H94O15 | DGDG(36:1) | 22.88 |
| 984.6 | C53H90O15 | DGDG(38:5) | 7.44 |
| 932.6 | C49H86O15 | DGDG(34:3) | 5.58 |
| 954.6 | C51H84O15 | DGDG(36:6) | 4.87 |
| MGDG | | | |
| 796.6 | C45H78O10 | MGDG(36:4) | 286.61 |
| 794.5 | C45H76O10 | MGDG(36:5) | 170.49 |
| 798.6 | C45H80O10 | MGDG(36:3) | 153.29 |
| 792.5 | C45H74O10 | MGDG(36:6) | 91.86 |
| 800.6 | C45H82O10 | MGDG(36:2) | 33.08 |
| 774.6 | C43H80O10 | MGDG(34:1) | 19.13 |
| 826.6 | C47H84O10 | MGDG(38:3) | 13.98 |
| 772.6 | C43H78O10 | MGDG(34:2) | 9.17 |
| PG | | | |
| 768.5 | C40H79O10P | PG(34:0) | 3.71 |
| 766.5 | C40H77O10P | PG(34:1) | 3.30 |
| 764.5 | C40H75O10P | PG(34:2) | 3.11 |
| 740.5 | C38H75O10P | PG(32:0) | 2.23 |
| 788.5 | C42H75O10P | PG(36:4) | 1.82 |
| LysoPG | | | |
| 526.3 | C24H45O9P | LPG(18:2) | 26.75 |
| 528.3 | C24H47O9P | LPG(18:1) | 20.15 |
| 500.3 | C22H43O9P | LPG(16:1) | 15.72 |
| 502.3 | C22H45O9P | LPG(16:0) | 14.98 |
| 524.3 | C24H43O9P | LPG(18:3) | 11.47 |
| LysoPC | | | |
| 520.3 | C26H50O7PN | LPC(18:2) | 8.32 |
| 522.3 | C26H52O7PN | LPC(18:1) | 5.67 |
| LysoPE | | | |
| 478.3 | C23H44O7PN | LPE(18:2) | 1.27 |
| 454.3 | C21H44O7PN | LPE(16:0) | 0.43 |
| 452.3 | C21H42O7PN | LPE(16:1) | 0.37 |
| PC | | | |
| 758.6 | C42H80O8PN | PC(34:2) | 7.79 |
| 782.6 | C44H80O8PN | PC(36:4) | 4.77 |
| 784.6 | C44H82O8PN | PC(36:3) | 2.48 |
| 760.6 | C42H82O8PN | PC(34:1) | 2.32 |
| 786.6 | C44H84O8PN | PC(36:2) | 1.08 |
| 756.5 | C42H78O8PN | PC(34:3) | 0.93 |
| 780.5 | C44H78O8PN | PC(36:5) | 0.78 |
| PE | | | |
| 716.5 | C39H74O8PN | PE(34:2) | 1.92 |

| 740.5 | C41H74O8PN | PE(36:4) | 1.44 |
| 742.5 | C41H76O8PN | PE(36:3) | 0.22 |
| 828.6 | C47H90O8PN | PE(42:2) | 0.21 |
| 718.5 | C39H76O8PN | PE(34:1) | 0.20 |
| PI | | | |
| 852.5 | C43H79O13P | PI(34:2) | 16.28 |
| 876.5 | C45H79O13P | PI(36:4) | 7.98 |
| 854.5 | C43H81O13P | PI(34:1) | 4.37 |
| 878.5 | C45H81O13P | PI(36:3) | 4.08 |
| 850.5 | C43H77O13P | PI(34:3) | 3.44 |
| 824.5 | C41H75O13P | PI(32:2) | 2.65 |
| 874.5 | C45H77O13P | PI(36:5) | 2.50 |
| 828.5 | C41H79O13P | PI(32:0) | 1.99 |
| 822.5 | C41H73O13P | PI(32:3) | 1.91 |
| PS | | | |
| 872.6 | C48H90O10PN | PS(42:2) | 8.61 |
| 760.5 | C40H74O10PN | PS(34:2) | 2.75 |
| 844.6 | C46H86O10PN | PS(40:2) | 1.61 |
| 900.7 | C50H94O10PN | PS(44:2) | 1.35 |
| 874.6 | C48H92O10PN | PS(42:1) | 0.93 |
| 870.6 | C48H88O10PN | PS(42:3) | 0.64 |
| 786.5 | C42H76O10PN | PS(36:3) | 0.54 |
| 784.5 | C42H74O10PN | PS(36:4) | 0.49 |
| PA | | | |
| 690.5 | C37H69O8P | PA(34:2) | 325.56 |
| 714.5 | C39H69O8P | PA(36:4) | 219.54 |
| 716.5 | C39H71O8P | PA(36:3) | 130.51 |
| 692.5 | C37H71O8P | PA(34:1) | 70.04 |
| 718.5 | C39H73O8P | PA(36:2) | 39.98 |
| 688.5 | C37H67O8P | PA(34:3) | 20.51 |
| 712.5 | C39H67O8P | PA(36:5) | 19.07 |
| 666.5 | C35H69O8P | PA(32:0) | 2.43 |
| DAG | | | |
| 34:2 | C37H72O5N | 18:2/16:0 | 68810.79 |
| 34:1 | C37H74O5N | 18:1/16:0 | 12404.35 |
| 36:4 | C39H72O5N | 18:2/18:2 | 7971.51 |
| 34:3 | C37H70O5N | 18:3/16:0 | 7154.70 |
| 36:3 | C39H74O5N | 18:2/18:1 | 5916.98 |
| 36:2 | C39H76O5N | 18:2/18:0 | 1695.15 |
| 36:4 | C39H72O5N | 18:3/18:1 | 1688.38 |
| 36:5 | C39H70O5N | 18:3/18:2 | 1203.29 |
| 36:2 | C39H76O5N | 18:1/18:1 | 1163.96 |
| 34:3 | C37H70O5N | 18:2/16:1 | 401.01 |
| 32:0 | C35H72O5N | 16:0/16:0 | 365.18 |
| 36:1 | C39H78O5N | 18:1/18:0 | 251.94 |
| 36:3 | C39H74O5N | 18:3/18:0 | 124.73 |
| 34:2 | C37H72O5N | 18:1/16:1 | 118.98 |
| 32:1 | C35H70O5N | 16:0/16:1 | 118.12 |
| 34:7-O | C37H62O6N | 18:3/dnOPDA | 82.71 |
| 34:4 | C37H68O5N | 18:2/16:2 | 82.62 |
| 36:6 | C39H68O5N | 18:3/18:3 | 79.35 |
| 34:4 | C37H68O5N | 18:3/16:1 | 52.67 |

| 34:5 | C37H66O5N | 18:2/16:3 | 40.19 |
|---|---|---|---|
| 34:3 | C37H70O5N | 18:1/16:2 | 34.97 |
| 36:7-O | C39H66O6N | OPDA/18:3 | 22.89 |
| 34:1 | C37H74O5N | 18:0/16:1 | 15.23 |
| 34:2 | C37H72O5N | 18:0/16:2 | 15.02 |
| 34:6 | C37H64O5N | 18:3/16:3 | 13.84 |
| 34:4 | C37H68O5N | 18:1/16:3 | 13.17 |
| 34:7-O | C37H62O6N | OPDA/16:3 | 11.43 |
| 34:5 | C37H66O5N | 18:3/16:2 | 9.84 |
| 34:8-2O | C37H60O7N | OPDA/dnOPDA | 4.68 |
| 34:3 | C37H70O5N | 18:0/16:3 | 4.61 |
| TAG | | | |
| 896.76807 | C57H102O6N | TAG(54:6) | 7.01 |
| 894.75247 | C57H100O6N | TAG(54:7) | 2.91 |
| 898.78367 | C57H104O6N | TAG(54:5) | 2.70 |
| 872.76807 | C55H102O6N | TAG(52:4) | 2.52 |
| 894.75247 | C57H100O6N | TAG(54:7) | 1.86 |
| 898.78367 | C57H104O6N | TAG(54:5) | 1.76 |
| 872.76807 | C55H102O6N | TAG(52:4) | 1.56 |
| 896.76807 | C57H102O6N | TAG(54:6) | 0.98 |
| 896.76807 | C57H102O6N | TAG(54:6) | 0.97 |
| 892.73687 | C57H98O6N | TAG(54:8) | 0.82 |
| 900.79927 | C57H106O6N | TAG(54:4) | 0.81 |
| 870.75247 | C55H100O6N | TAG(52:5) | 0.63 |
| 874.78367 | C55H104O6N | TAG(52:3) | 0.62 |
| 874.78367 | C55H104O6N | TAG(52:3) | 0.61 |
| 874.78367 | C55H104O6N | TAG(52:3) | 0.54 |
| 900.79927 | C57H106O6N | TAG(54:4) | 0.53 |
| 848.76807 | C53H102O6N | TAG(50:2) | 0.50 |
| 870.75247 | C55H100O6N | TAG(52:5) | 0.42 |
| 892.73687 | C57H98O6N | TAG(54:8) | 0.36 |
| 848.76807 | C53H102O6N | TAG(50:2) | 0.23 |
| 872.76807 | C55H102O6N | TAG(52:4) | 0.23 |
| 898.78367 | C57H104O6N | TAG(54:5) | 0.22 |
| 850.78367 | C53H104O6N | TAG(50:1) | 0.19 |
| 872.76807 | C55H102O6N | TAG(52:4) | 0.19 |
| 894.75247 | C57H100O6N | TAG(54:7) | 0.17 |
| 876.79927 | C55H106O6N | TAG(52:2) | 0.17 |
| 902.81487 | C57H108O6N | TAG(54:3) | 0.16 |
| 900.79927 | C57H106O6N | TAG(54:4) | 0.13 |

**Figure S7. Measurement of lipid oxidation, Related to Figure 2.**
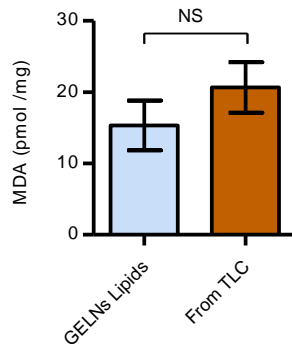


Lipid oxidation of GELNs total lipids and lipids extracted from TLC was measured by level of malondialdehyde (MDA). The lipid sample was mixed with TBA reagent and kept at boiling water bath for 15 min and read at 535 nm. The concentration of MDA was calculated by standard MDA. Results are expressed as mean ± standard deviation from three independent experiments. Student 't' Test was used for analysis of statistical significance. NS; Not significant.

**Figure S8. Characterization of GELNs lipid nano particles, Related to Figure 3.**
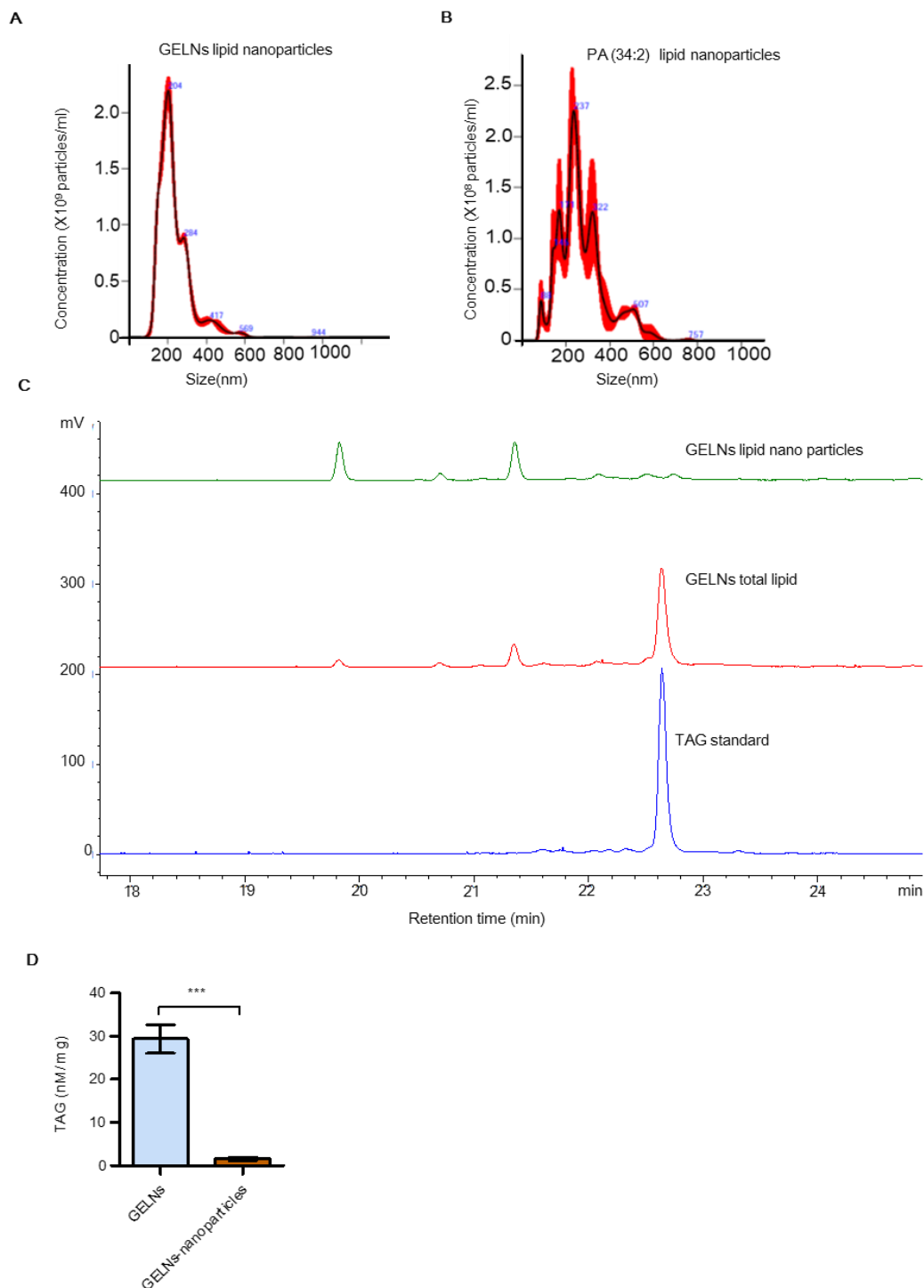


Lipid nanoparticles were made from LipidG and PA (34:2). Size distribution lipid nanoparticles were determined using a NanoSight NS300 (Westborough, MA) with a flow speed at 0.03 mL per min. **(A)** size distribution of GELNs lipid nanoparticles. **(B)** size distribution of PA (34:2) lipid nanoparticles. **(C-D)** TAG content in GELNs lipid nanoparticles was determined by HPLC. TAG levels were expressed as mean ± standard deviation from three independent experiments. Student 't' test was used to analysis statistical significance of TAG level between GELNs total lipid vs GELNs lipid nanoparticles.***P<0.001.

**Table S5. GELN-binding proteins of *P. gingivalis*, Related to Figure 5.**

| Identified Proteins | Gene Symbol | Accession Number | Molecular Weight |
|---|---|---|---|
| Lys-gingipain | *kgp* | KGP_PORG3 | 187 kDa |
| Hemagglutinin | *hagA* | B2RLK7_PORG3 | 283 kDa |
| Receptor antigen B | *ragB* | B2RHG8_PORG3 | 57 kDa |
| Cluster of Gingipain R1 | *rgpA* | CPG1_PORG3 | 185 kDa |
| Receptor antigen A | *ragA* | B2RHG7_PORG3 | 115 kDa |
| 35 kDa hemin binding protein | *HBP35* | B2RII3_PORG3 | 38 kDa |
| Peptidylarginine deiminase | PGN_0898 | B2RJ72_PORG3 | 62 kDa |
| Immunoreactive 61 kDa antigen | *tapA* | B2RH26_PORG3 | 61 kDa |
| C-terminal domain of Arg-and Lys-gingipain proteinase | *rgpA_4* | B2RHG9_PORG3 | 32 kDa |
| Uncharacterized protein | PGN_0654 | B2RIH8_PORG3 | 35 kDa |
| Zn-carboxypeptidase | *scpD* | B2RHK9_PORG3 | 92 kDa |
| Minor fimbrial subunit Mfa1 | *mfa1* | MFA1_PORG3 | 61 kDa |
| T9SS C-terminal target domain-containing protease | PGN_0458 | B2RHY2_PORG3 | 57 kDa |
| Glyceraldehyde-3-phosphate dehydrogenase | *gapA* | B2RH47_PORG3 | 36 kDa |
| NAD-specific glutamate dehydrogenase | *gdh* | DHE2_PORG3 | 49 kDa |
| Uncharacterized protein | PGN_0129 | B2RH03_PORG3 | 22 kDa |
| Outer membrane lipoprotein immunoreactive 42 kDa antigen PG33 | *ompA_3* | B2RIQ3_PORG3 | 43 kDa |
| Fibronectin type III domain protein | *fib3* | B2RIW9_PORG3 | 79 kDa |
| UDP-N-acetylenolpyruvoylglucosamine reductase inner membrane lipoprotein | PGN_1129 | B2RJV3_PORG3 | 17 kDa |
| Lipoprotein | PGN_0426 | B2RHV0_PORG3 | 17 kDa |
| Lysyl endopeptidase | *pepK* | B2RKP0_PORG3 | 103 kDa |
| Outer membrane lipoprotein immunoreactive 42 kDa antigen PG33 | *ompA_2* | B2RIQ2_PORG3 | 42 kDa |
| Uncharacterized protein | PGN_1557 | B2RL31_PORG3 | 30 kDa |
| Ferric enterobactin receptor | *pfeA_1* | B2RIK7_PORG3 | 79 kDa |

**Figure S9. Schematic representation GELNs miRNAs targeting genes in *P. gingivalis*, Related to Figure 5 and Figure 6.**

1      5112

(2217−2223) (2450−2458) (2849−2842) (3085−3091) (1024−1030) (4136−4129)

5'- ▬ -3'

rgpA(PGN_1970)   TTTGGAT   TTTGGATTG   TTTGGATT   TTTGGATT   TTTGGAT   GGATTGAA

     | | | | | | |   | | | | | | | |   | | | | | | | |   | | | | | | | |   | | | | | | |   | | | | | | | |

aly-miR159a-3p   TTTGGAT   TTTGGATTG   TTTGGATT   TTTGGATT   TTTGGAT   GGATTGAA


1      2211

(352 - 356)

5'- ▬ -3'

rgpB (PGN_1466)   AGGGAGC

     | | | | | | | |

aly-miR159a-3p   AGGGAGC


1      5172

(408−414) (555−562) (891−897) (1598−1604) (3145−3151) (3969−3975)

5'- ▬ -3'

kgp (PGN_1728)  GAAGGGA   ATTGAAG   TGGATTG   TTGAAGG   TTGGATT   TTTGGAT

     | | | | | | |   | | | | | | |   | | | | | | |   | | | | | | |   | | | | | | |   | | | | | | |

aly-miR159a-3p  GAAGGGA   ATTGAAG   TGGATTG   TTGAAGG   TTGGATT   TTTGGAT


1      7887

(2776−2783) (2857−2864) (4144−4151) (4225−4232)

5'- ▬ -3'

Hemagglutinin (HagA)   GGATTGAA   TTTGGATT   GGATTGAA   TTTGGATT

(PGN_1733)       | | | | | | | |   | | | | | | | |   | | | | | | | |   | | | | | | | |

aly-miR159a-3p   GGATTGAA   TTTGGATT   GGATTGAA   TTTGGATT


1    849          1    900

(495 - 504)          (477 - 484)

5'- ▬ -3'          5'- ▬ -3'

AraC family transcriptional   TTTGGATT      AraC family transcriptional   TCTCGGAC

regulator(PGN_0082)   | | | | | | | |      regulator(PGN_0205)   | | | | | | | |

aly-miR159a-3p   TTTGGATT          gma-miR166u   TCTCGGAC


1      2676

(159−166) (200−206) (460−466) (609−618) (776−783) (1024−1030) (1318−1324) (1508−1514)

5'- ▬ -3'

outer membrane   TCATTCCC  CAGGCTT  CTTCATT  TTCATTCCCC  TCGGACCA  CTTCATT  ATTCCCC  TCATTCC

protein (PGN_0299)  | | | | | | | |  | | | | | | |  | | | | | | |  | | | | | | | | | |  | | | | | | | |  | | | | | | |  | | | | | | |  | | | | | |

gma-miR166p   TCATTCCC  CAGGCTT  CTTCATT  TTCATTCCCC  TCGGACCA  CTTCATT  ATTCCCC  TCATTCC
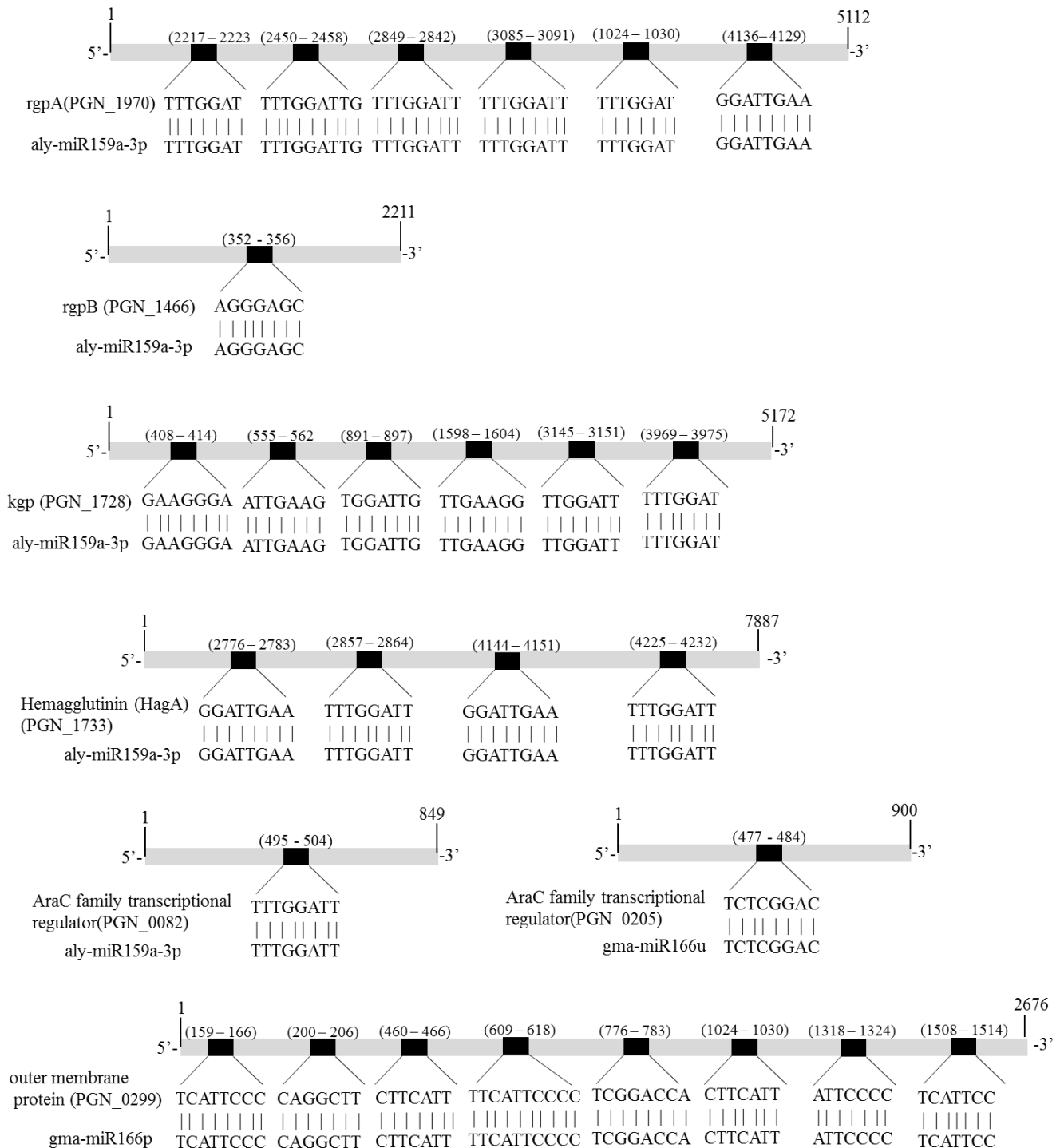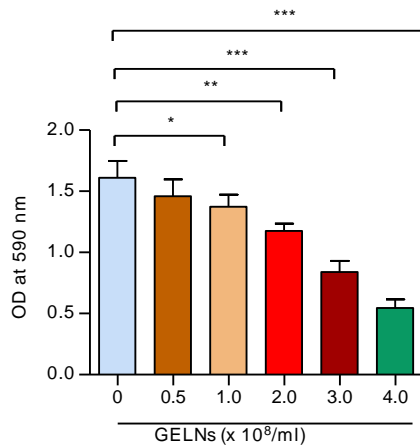
**Figure. S10. GELNS inhibit biofilm formation of *P. gingivalis*,** Related to Figure 8.



Human saliva was coated in 96-well plate for overnight. *P. gingivalis* was treated with different concentration (0- $4.0 \times 10^8$ particles/ml) of GELNS and incubated at anaerobic chamber for 24 h. Then, bacteria were removed by washing with PBS and the biofilm was stained with 0.5% of crystal violet for 15 min. Excess staining was removed by washing and 99% ethanol added. Optical density was measured at 590 nm. Results are expressed as means with standard deviation from three independent experiments. * P <0.05, **P<0.01, ***P<0.001 compared with control group using Student 't' Test.

**Figure S11. GELNs significantly decreased pro-inflammatory cytokine expression in *P. gingivalis* infected mice, Related to Figure 8.**
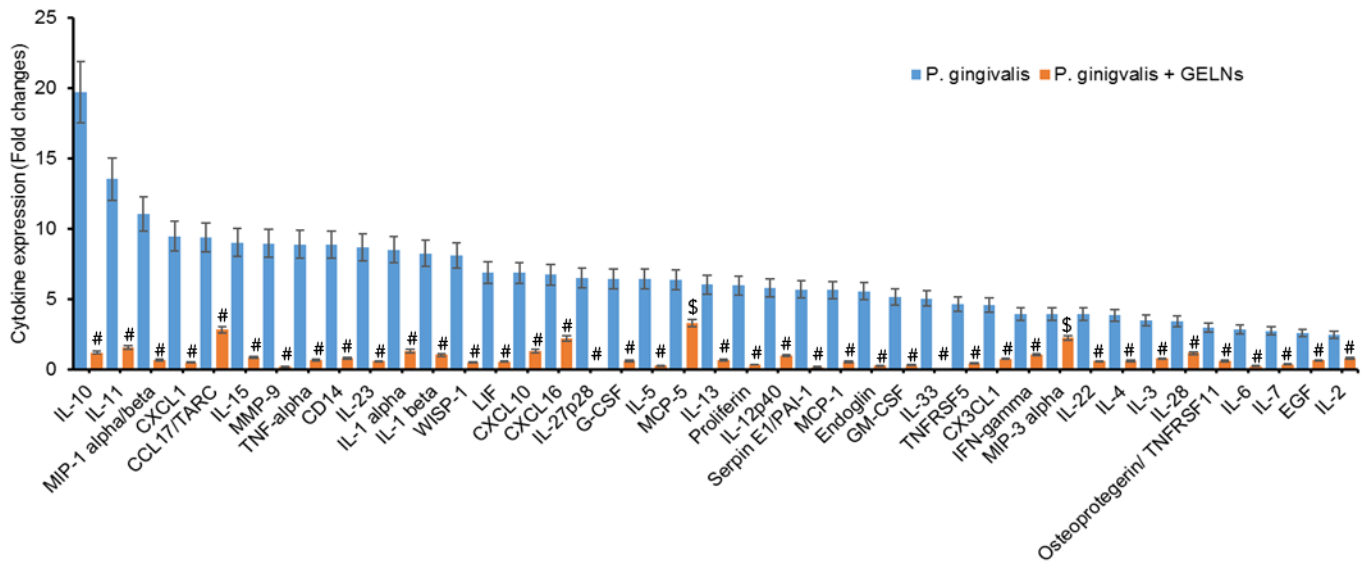


Cytokine expression was determined by a cytokine array. Plasma was collected from control, *P. gingivalis* infected and *P. gingivalis* infected with GELN treated mice. The cytokines levels are expressed as mean ± standard deviation from three independent experiments. Student 't' test was used to analysis statistical significance of cytokine level between P. gingivalis infected Vs GELNs treatments. $^{\$}P<0.01$, $^{\#}P<0.001$.

**Table S6. Primers list, Related to Figure 5, Figure 6, Figure 7 and Figure 8**

| Primer Name | Forward | Reverse |
|---|---|---|
| AraC | CGCGAACTCTTCTGCATCTT | GAATACGAAGGCACGAAAGC |
| OMP | GGATCGTTCGCTTCAGATGT | AGCCATGATGGAAATTTTGG |
| RodA | CGATTATAAGGGACGGATCG | CCATCATGAAAAGGTGGGATA |
| HA | GATCGATGCTGATGGTGATG | CCGCTAGCAGTCCATGATTT |
| porX | GATCGGGGACAGAAGTACCA | ATTCGGGTAGGCGAAGAAGT |
| porY | AGAATTGAGGATGCCGAATG | TGCATACGAGCCTTTCTCCT |
| porL | GGGTGCTCTCTTCAAGTTGC | TCCATCGGATTCTTCGAGTC |
| porM | TTCCGTCACAGCTCAATCAG | ATTTCACGCTTACCCAAACG |
| porN | TCGCTCGTGAACGAGTAATG | GAATCGGGCGTAGGACAGTA |
| porK | AGCTCAATCCGGATCAAATG | GATGATATTGCCGCTTTCGT |
| porW | CTCAGTCCGGACAGGAGAAG | CTGCAGGAAATCGGCATTAT |
| sov | AGGCGGCAGAGACTATGAAA | CTGATAAACCTGCCCGTTGT |
| porQ | ATGCGTTTCCTGAACTACGG | CACCAAGGCCAAAGGAACTA |
| porP | AGCTACTGACGGGCACAGTT | AAAGCATAGCCGGCATAGAA |
| porT | GGTCTCGGATGCGATTTTTA | CTCGAAATTGAACGTGAGCA |
| porV | CTCTGTGCCATCGCTGAATA | AGAAACCGGTCATCTGCATC |
| OMPA2 | CATTGACATTGCAGGTGGAG | TCGAACATGAAGTCGAGGTG |
| fimA | TTGTTGGGACTTGCTGCTCTTG | TTCGGCTGATTTGATGGCTTCC |
| 16S rRNA | AGGAACTCCGATTGCGAAGG | TCGGTTTACTGCGTGGACTACC |
| IL-1β | GTTCCCATTAGACAACTGC | GATTCTTTCCTTTGAGGC |
| IL-6 | GATACCACTCCCAACAGACC | GCAATGGCAATTCTGATTGT |
| TNF-α | TCTATGGCCCAGACCCTCAC | GACGGCAGAGAGGAGGTTGA |
| GAPDH | AGGTCATCCCAGAGCTGAACG | ACCCTGTTGCTGTAGCCGTAT |

## Transparent Methods

### Bacterial strains and growth condition

 *P. gingivalis* 33277 was cultured in trypticase soy broth supplemented with yeast extract (1 mg/ml), hemin (5 µg/ml) and menadione (1 µg/ml) and incubated at 37°C in an anaerobic chamber (85%$N_2$, 10%$H_2$, 5%$CO_2$). *S. gordonii* DL1 was cultured in brain-heart infusion broth containing 0.5% yeast extract and incubated anaerobically at 37°C.

A *P. gingivalis* 33277 deletion mutation in *HBP35* (PGN_0659) was obtained by allelic replacement. Briefly, DNA sequences 999 bp upstream of the PGN_0659 ATG initiation codon and 930 bp downstream of the PGN_0659 TGA stop codon were amplified using the 0659usF- GATGAGCCGACGATGAGTATGC, 0659usR GAAGCTATCGGGGGGTACCTTGCAAATACTTTGCCTCTGTTATCGTC and 0659dsF TGTCCCTGAAAAATTTCATCCTATTGAGCTAAGATTTAAACGAAAACTGCG, 0659dsR AATGCTCGGTTTCAGTGTCTGC primers, respectively, using *P. gingivalis* 33277 genomic DNA. An *ermF* cassette was amplified from *P. gingivalis* 33277△*ltp1* as described earlier (Simionato et al., 2006) using the ermF GGTTACCCCCGATAGCTTCC and ermR GGATGAAATTTTTCAGGGACA primers that contained 5' homology with the 0659usR and 0659dsF primers. The final PCR fusion product was purified using the New England Biolabs Monarch PCR and DNA cleanup kit. The amplicon was directly electroporated into *P. gingivalis* 33277 (Simionato et al., 2006). Recombinants were selected using TSB blood agar plates supplemented with yeast extract, hemin, menadione and erythromycin (10 ug/mL). Replacement of PGN_0659 was confirmed by real-time PCR using the following primers 0659-F - TACTCTCTGCTGCTATCCTAAGT and 0659-R CCTCCAACACCACATTCTTCT; 0658-F- GCTTCCGGTAGCGATGATAA and 0658R- CACCTCCACATACTCGTCATAC; 0660-F- TGGCTTATCGTGGCTCTTTC and 0660-R- GGAGGATCTCTTCTGCATCAC.

To measure the effect of GELNs on growth, *P. gingivalis* and *S. gordonii* were cultured over 0-48 h in the presence or absence of different concentrations of GELNs (0-6.0 × $10^8$ particles/ml) and

total lipids derived from these particles (LipdG) (see below). *P. gingivalis* and *S. gordonii* growth was determined by measuring optical density at 600 nm.

**Culture of TIGK cells**

Human telomerase immortalized keratinocytes (TIGKs) derived from the human gingival epithelium were maintained at 37°C and 5% $CO_2$ in Dermalife-K serum free culture medium (Lifeline Cell Technology, Carlsbad, CA).

**Isolation and purification of ginger exosome-like nanoparticles (GELNs)**

Ginger exosome-like nanoparticles (GELNs) were isolated and purified. Ginger was purchased from a local supermarket and washed with sterile PBS and the skin peeled away. Ginger was ground in a blender to obtain the juice and strained to remove the larger particles. Juice was sequentially centrifuged at 1000g for 10 min, 3000g for 20 min and 10,000g for 40 min to remove particles. The supernatant was then centrifuged at 150,000g for 2 h, the pellet was resuspended in sterile PBS and transferred to a sucrose step gradient (8%/15%/30%/45%/60%), followed by centrifugation at 150,000g for 2 h at 4°. The bands between the 8%/30% layer and 30%/45% layer were harvested separately and noted as ginger exosome-like nanoparticles (GELNs). The purified GELNs were fixed with 2% paraformaldehyde and imaged by electron microscopy (Zeiss EM 900). GELN size and concentration (particle number) was determined using a NanoSight NS300 (Malvern Instrument, UK) at a flow rate of 30 µl per minute. GELNs were also isolated from a commercially available ginger supplement (Super pure Ginger, The Synergy Company) after ginger supplement was suspended in PBS with the same procedure as described above.

**GELN uptake assay**

Bacterial uptake of GELNs was quantified by flow cytometry. In brief, *P. gingivalis* and *S. gordonii* were labelled with PKH67 (green) and GELNs were labelled with PKH26 (red) according to the manufacturer's protocol (Sigma). Fluorescent labeled bacteria ($1 \times 10^8$) were incubated with fluorescent labeled GELNs (0- $6.0 \times 10^8$ particles) for 1 h at 37°C in an an anaerobic chamber. The percentage of GELNs taken up by *P. gingivalis* or *S. gordonii* was quantified by flow cytometry.

**Confocal microscopy**

The interaction or uptake of GELNs by *P. gingivalis* was determined by confocal microscopy. Briefly, *P. gingivalis* and GELNs were labelled with PKH67 (green) and PKH26 (red), respectively, according to the manufacturer's protocol (Sigma). Fluorescent labeled *P. gingivalis* ($1 \times 10^8$) was incubated with fluorescent labeled GELNs ($6.0 \times 10^8$ particles) for 1 h at 37°C. The interaction of *P. gingivalis* and GELNs was visualized by confocal microscopy (Nikon).

## *P. gingivalis* invasion of epithelial cells

*P. gingivalis* invasion into oral epithelial cells was determined by an antibiotic protection assay *P. gingivalis* was grown to mid-log phase and incubated at 37°C for 3 h with or without GELNs ($4.0 \times 10^8$ particles). Cells were collected by centrifugation for 10 min at 5000g and infected into TIGK cells at a MOI of 10 at 37°C for 1 h. Unbound bacteria were removed by washing with PBS and surface attached external non-invading bacteria were killed by incubation with gentamicin (300 µg/ml) and metronidazole (200 µg/ml) for 4 h. TIGK cells were washed with PBS and lysed with sterile distilled water. Intracellular *P. gingivalis* were plated, incubated anaerobically at 37°C for 7 days and CFUs determined. For the proliferation assay, after antibiotic treatment, cells were further incubated anaerobically for 24 h. RNA was extracted and subjected to real time PCR for 16s rRNA expression. The number of *P. gingivalis* was calculated using a standard curve derived from a known amount of *P. gingivalis*.

## *P. gingivalis* attachment to epithelial cells

The amount of *P. gingivalis* attaching to the surface of gingival epithelial cells was determined. TIGK cells were cultured in 96-well plates for 24 h and fixed with 5% buffered formalin for 1 h, *P. gingivalis* treated with and without GELNs (as above) were reacted with the TIGK cells at a MOI of 10 for 1 h at 37°C. Cells were washed with PBS to remove non-adherent bacteria and incubated with *P. gingivalis* whole-cell antibodies (1:10,000) for 1 h at 37°C. After washing, binding was detected with a secondary horse radish peroxidase (HRP)-anti-rabbit antibody (1:5,000) with 3,3′,5,5′-tetramethylbenzidine substrate (Sigma), and the results at 450 nm recorded.

For confocal microscopy, the secondary antibody for *P. gingivalis* was Alexa 568-conjugated IgG (1: 5000). Nuclear staining was performed with DAPI for 15 min and localization of *P. gingivalis* was visualized by confocal microscopy (Nikon).

**Gingipain proteolytic activity**

The proteolytic activity of arginine-specific (Rgp) and lysine specific (Kgp) gingipain was measured. *P. gingivalis* was cultured to mid-log phase and treated with and without GELNs (2.0-4.0 × 10^8 particles /ml) for 6 h. The bacterial cells were collected by centrifugation at 5000g for 10 min, washed and lysed with Bugbuster reagent (Millipore Sigma, Burlington, MA, USA). The chromogenic *p*-nitroanillide substrates N-benzoyl-L-arginine-pNA or toluenesulfonyl-glycyl-prolyl-L-lysine-pNA (Sigma) were used to measure RgpA/B and Kgp, respectively. Bacterial cell lysates (50 μl) were pre-incubated with assay buffer (200 mM Tris-HCl, 5 mM CaCl$_2$, 150 mM NaCl and supplemented with 10 mM cysteine) in a 96-well plate and 0.5 mM of specific substrate was added to each well. The rate of substrate hydrolysis and accumulation of p-nitroanillide was monitored spectrophotometrically at 405 nm. The enzyme activity was calculated and given as mOD/min/μl.

**RNA isolation and quantitative real time PCR (qRT-PCR)**

Total RNA was isolated from *P. gingivalis* and TIGK cells using TRIzol reagent according to the manufacturer's protocol (Invitrogen). RNA (1 μg) was converted into cDNA with an iScript cDNA synthesis kit (Bio-Rad, Hercules, CA). cDNA samples were amplified with Sso Fast green super mix in CFX96 Real–time PCR system (Bio-Rad). mRNA expression was quantified by the ΔΔCt method using 16 S rRNA expression as an internal control for bacterial gene expression and GAPDH expression as an internal control for mouse and human gene expression. All primers were purchased form Eurofins MWG Operon and primers are listed in Supplementary Table 6.

**Western blot**

*P. gingivalis* was incubated anaerobically at 37°C for 6 h with or without GELNs (0-4.0 × 10^8 particles /ml). Total cell lysates were prepared in Bugbuster lysis reagent with protease and phosphatase inhibitors (Roche). Cell lysates were separated by SDS-PAGE (4- 15% gradient gel) and transferred onto nitrocellulose membranes. After transfer, membranes were probed with primary polyclonal antibodies specific for FimA or Mfa1 at 1:1000 for 1 h at room temperature. The membrane was incubated with secondary antibodies conjugated to Alex-647 (Eugene, OR, USA) at 1:10,000 for 1 h at room temperature. Bands were visualized and analyzed based on band intensity on an Odyssey Imager (Licor Inc, Lincoln, NE, USA).

**Lipid extraction and TLC analysis**

Total lipids from GELNs were extracted with chloroform:methanol (2:1, v/v). GELNs was mixed with chloroform:methanol and vortex the mixture. Centrifuge at 2000 xg for 10 min and carefully remove bottom layer contains lipids and dried under nitrogen. Then, thin layer chromatography (TLC) was performed. HPTLC-plates (silica gel 60 with concentrating zone, 20 cm × 10 cm; Merck) were used for the separation. Aliquots of concentrated lipid samples extracted from GELNs were separated on HPTLC-plates and the plates developed with chloroform:methanol:$H_2O$ (65:25:4). After drying, lipids were stained using iodine vapor. The plate was imaged with an Odyssey Scanner.

**Lipid oxidation measurement:** Lipid oxidation was measured by quantification of malondialdehyde (MDA) 200 μl of lipids derived from GELNs and GELN lipids extracted from TLC plates were mixed with 400 μl of TBA reagent containing Trichloroacetic acid (15%), HCl (0.2N), thiobarbuitric acid (0.37%) with 0.03% butylated hydroxytoluene (BHT). The sample was kept in boiling water bath for 15 min and samples cooled down to room temperature. The samples were centrifuged for 10 min at 1000g. The absorbance of the solution at 535 nm was determined. The concentration of MDA was calculated using standard MDA.

**Lipidomic analysis**

Lipid samples extracted from GELNs were submitted to the Lipidomics Research Center, Kansas State University (Manhattan, KS) for analysis. The lipid composition was determined using a triple quadrupole mass spectrometer (Applied Biosystems Q-TRAP, Applied Biosystems, Foster City, CA). The data are reported as concentration (nmol/mg GELNs) and percentage of each lipid in total signal for the molecular species determined after normalization of the signals to internal standards of the same lipid class.

**Preparation of GELN RNA libraries and sequencing**

Small RNA libraries were generated with 100 ng of total RNA from GELNs and TruSeq Small RNA Library Preparation Kits (Illumina) according to the manufacturer's instructions. Following PCR amplification (16 cycles), libraries between 140 and 160 bp in size were gel purified and resuspended in ultrapure water (11 μl). Equal amounts of libraries were pooled and sequenced

on an Illumina HiSeq 2500, followed by demultiplexing and fastq generation with CASAVA v1.8.4. Raw fastqs were adapter and quality score trimmed with cut adapt v1.10. with a minimum length of 15 nucleotides. MicroRNAs were identified using the sRNABench Pipeline (version 05/14). A core set of plant miRNAs from miRBase v21 was used as a reference and this set included all 14 plant species with at least 200 mature microRNA sequences annotated in miRBase. Within the sRNABench pipeline, mapping was performed with bowtie (v0.12.9) and microRNA folding was predicted with RNAfold using the Vienna package (v2.1.6).

**Delivery of miRNA into *P. gingivalis***

GELNs miRNAs aly-miR-159a-3p, gma-miR166u, gma-miR166p and gma-miR319a were packaged into lemon-derived lipid nanoparticles. Total lipids were extracted from lemon-derived exosome-like nanoparticles. 20 nM of miRNA was added to 100 nM of lemon lipids in 0.9% NaCl and PEI (2 µg/ml), and this mixture was sonicated in a water bath to make a lipid nanoparticles-miRNA complex. The complex was centrifuged at 36,000 rpm for 1 h and the unbound RNA content in the supernatant was measured. *P. gingivalis* was treated with the RNA bound lipid nanoparticles for 24 h.

**2DLC-MS/MS analysis and its data analysis**

*P. gingivalis* was incubated anaerobically with PBS in the presence or absence of GELNs ($4.0 \times 10^8$ particles/ml) for 24 h. Bacterial media was collected by centrifugation and filtered (0.22 µm) to remove bacterial cells. To extract polar metabolites for 2DLC-MS/MS analysis, 500 µL of culture medium was lyophilized, then redissolved in 100 µL 20% acetonitrile. After 3 min of vigorous vortex mixing, the sample was centrifuged at 12,000g at 4°C for 20 min. The supernatant was collected and used for 2DLC-MS/MS analysis.

All samples were analyzed on a Thermo Q Exactive HF Hybrid Quadrupole-Orbitrap Mass Spectrometer coupled with a Thermo DIONEX UltiMate 3000 HPLC system (Thermo Fisher Scientific, Waltham, MA, USA). The UltiMate 3000 HPLC system was equipped with a hydrophilic interaction chromatography (HILIC) column and a reverse phase chromatography (RPC) column. The HILIC column was a SeQuant® ZIC®-cHILIC HPLC column (150 × 2.1 mm i.d., 3 µm) purchased from Phenomenex (Torrance, CA, USA). The RPC column was an ACQUITY UPLC

HSS T3 column (150 × 2.1 mm i.d., 1.8 μm) purchased from Waters (Milford, MA, USA). The two columns were configured in parallel 2DLC mode.

For 2DLC separation, the mobile phase A for RPC was water with 0.1% formic acid and the mobile phase A for HILIC was 10 mM ammonium acetate (pH adjusted to 3.25 with acetate). Both RPC and HILIC used the same mobile phase B, acetonitrile with 0.1% formic acid. The RPC gradient was 0 min, 5% B, hold for 5.0 min; 5.0 min to 6.1 min, 5% B to 15% B; 6.1 min to 10.0 min, 15% B to 60% B, hold for 2.0 min; 12.0 min to 14.0 min, 60% B to 100% B, hold for 13.0 min; 27.0 min to 27.1 min, 100% B to 5% B, hold for 12.9 min. The HILIC gradient was 0 to 5.0 min, 95% B to 35% B, hold for 1.0 min; 6.0 min to 6.1 min, 35% B to 5% B, hold for 16.9 min; 23.0 min to 23.1 min, 5% B to 95% B, hold for 16.9 min. The flow rate was 0.4 mL/min for RPC and 0.3 mL/min for HILIC. The column temperature was 40°C for both columns. The injection volume was 2 μL.

To avoid systemic bias, the samples were analyzed by 2DLC-MS in a random order. All samples were first analyzed by 2DLC-MS in positive mode followed by 2DLC-MS in negative mode to obtain the full MS data of each metabolite. For quality control purposes, a pooled sample was prepared by mixing a small portion of the supernatant from each sample and was analyzed by 2DLC-MS after injection of every six biological samples. The pooled sample was also analyzed by 2DLC-MS/MS in positive mode and negative mode to acquire MS/MS spectra for metabolite identification.

For 2DLC-MS data analysis, MetSign software was used for spectrum deconvolution, metabolite identification, cross-sample peak list alignment, normalization, and statistical analysis. To identify metabolites, the 2DLC-MS/MS data of pooled sample were first matched to our in-house MS/MS database that contains the parent ion m/z, MS/MS spectra, and retention time of 187 metabolite standards. The thresholds used for metabolite identification were MS/MS spectral similarity $\geq 0.4$, retention time difference $\leq 0.15$ min, and m/z variation $\leq 4$ ppm. The 2DLC-MS/MS data without a match in the in-house database were then analyzed using Compound Discoverer software (Thermo Fisher Scientific, Inc., Germany), where the threshold of MS/MS spectra similarity score was set as $\geq 40$ with a maximum score of 100. The remaining peaks that did not

have a match were then matched to the metabolites in our in-house MS database using the parent ion m/z and retention time. The thresholds for assignment using the parent ion m/z and retention time were $\leq$ 4 ppm and $\leq$ 0.15 min, respectively.

**Transmission Electron Microscopy**

*P. gingivalis* and *S. gordonii* were treated with PBS or GELNs (6.0 × $10^8$ particles/ml) for 3 h. Bacterial cells were collected by centrifugation (5000 g, 10 min) and resuspended in 10 mM Tris (pH7.8) and fixed with 2% formaldehyde and 1% glutaraldehyde. The bacterial suspension (20 μl) was applied to a formvar-coated copper grid (200 mesh, Electron Microscopy Science, PA), air dried and negatively stained with 0.5% ammonium molybdate. Bacterial morphology was observed with a transmission electron microscope (Thermo-Fisher TEM Tecnai Spirit) at 80 kV and images were collected with an AMT XR60 digital camera.

**Outer membrane permeability assay (EtBr influx assay)**

*P. gingivalis* was grown to mid-log phase and washed with binding buffer (25 mM MES pH 6.0, 25 mM NaCl). *P. gingivalis* was treated for 2 h at 37°C with or without GELNs (0- 6.0 ×$10^8$ particles/ml) and then ethidium bromide (0.5 μM) was added. The fluorescence of the Et-Br-nucleic acid complex was immediately measured in a fluorescence spectrophotometer (Molecular Device) with excitation and emission wavelengths of 545 and 600 nm, respectively. The widths of the slits were 5 and 10 nm, respectively.

**Cytoplasmic membrane integrity assay**

The cytoplasmic membrane depolarization of *P. gingivalis* was measured by using a membrane potential sensitive fluorescent dye diSC$_3$-5. Mid-logarithmic phase *P. gingivalis* was washed with 5 mM sodium HEPES buffer, pH 7.4, containing 20 mM glucose, and resuspended to an OD$_{600}$ of 0.05 in the same buffer. The cell suspension was incubated with 0.4 μM diSC$_3$ until a stable reduction of fluorescence was achieved. KCl was added to a final concentration of 0.1 M to equilibrate the cytoplasmic and external K$^+$ concentration. *P. gingivalis* was treated for 2 h at 37°C with or without GELNs (6.0 x $10^8$ particles /ml). Changes in fluorescence were recorded using an F-4500 fluorescence spectrophotometer (Hitachi, Japan) with an excitation wavelength of 622 nm and an emission wavelength of 670 nm.

**Lipid nanoparticles preparation**

Total GELN lipids were extracted with chloroform:methanol (2:1, v/v) Thin layer chromatography (TLC) was performed with a PA (34:2) standard. The corresponding PA band was excised from the TLC plate and the remaining bands were pooled together. GELN total lipids, PA depleted lipids and PA (34:2) were completely dried under a stream of nitrogen gas and overnight dry under vacuum. The lipid film was suspended in HBS running buffer (20 mM HEPES, 150 mM NaCl, pH 7.4), gently vortexed and sonicated for 10 min until a clear solution was formed. The lipid nanoparticle suspension was extruded through a polycarbonate membrane filter syringe with a pore size of 100 nm. The size of the lipid nanoparticles was confirmed using a NanoSight NS300 (Malvern Panalytical Inc, MA, USA). Total lipids were determined by measuring total phosphate level (Baginski et al., 1972).

**HPLC analysis of TAG**

Total lipids were extracted from GELNs and lipid nanopartilces made from GELNs lipid. The samples were dissolved in methanol and 10 µl of sample was injected for high-performance liquid chromatography (HPLC) analysis with 380 ELSD detection system (Agilent Technologies). The HPLC analysis was performed on an Agilent 1260 Infinity system equipped with an Agilent 300SB-C8 column (4.6 x 250 mm, 5 µm) connected to a guard column, with the following parameters: mobile phase A: water; mobile phase B: methanol; gradient: 10% B in first 5 min, increase to 95% B in 10 min, hold 95% B for 5 min and then back to 10 % B in 5 min; flow rate: 1.0 ml/min; Column temperature was controlled at 37°C. ELSD setting include evaporator temperature 30°C, nebulizer temperature 30°C, gas flow rate 1.2 SLM and 350 kPa for nitrogen pressure with flow rate was 1 ml/min. The standard glyceryl trinoleate (cat: T9517) was purchase from Sigma.

**Surface Plasmon Resonance (SPR)**

SPR experiments were conducted on an OpenSPR™ (Nicoya, Lifesciences, ON, CA). All experiments were performed on a LIP-1 sensor (Nicoya, Lifesciences). Tests were run at a flow rate of 20 µl/min using HBS running buffer (20 mM HEPES, 150 mM NaCl, pH 7.4). First, the LIP-1 sensor chip was cleaned with octyl β-D-glucopyranoside (40 mM) and CHAPS (20 mM). Liposomes (1 mg/ml) were injected on the sensor chip for 10 min until stable resonance was

obtained. After immobilization of lipid nanoparticles, the surface was blocked with BSA (3%) in running buffer. After a stable signal was obtained, *P. gingivalis* total cell lysates (5 µg/ml of protein) were run over the immobilized liposomes. A negative control test was also performed by injecting protein onto a blank sensor chip to check for non-specific binding. After 10 min, the lipid nanoparticle binding protein was eluted using NaOH (200 µM). The eluted protein was subjected to LC-MS proteomic analysis for identification of GELN lipid nanoparticles and PA binding proteins. The sensograms were analyzed using TraceDrawer kinetic analysis software.

**Lipid nanoparticle pull down assay**

GELN lipid interactions with HBP35 were further confirmed using a lipid nanoparticle pull down assay. GELN lipid nanoparticles were fluorescently labelled with PKH26 in vesicle buffer (50 mM Tris-HCl (pH 7.5) and 150 mM NaCl). The labelled nanoparticles were incubated with biotin-HBP35 peptide (100 µM) for 2 h at 4°C with rotation in vesicle buffer. The lipid-protein complex was pulled down by streptavidin magnetic beads. The complex was washed thoroughly and the presence of lipid nanoparticles in the complex confirmed by flow cytometer. The number of lipid nanoparticles in the complex was determined using a Nanosight 300 and the quantity of lipid nanoparticles was determined by fluorescence intensity measured in a fluorescence spectrophotometer (Molecular Device) with excitation and emission wavelengths of 551 and 567 nm, respectively.

**Proteomic sample preparation**

GELN binding proteins of *P. gingivalis* were identified by LC-MS proteomics. Briefly, GELNs were labelled with biotin using an EZ-Link™ Sulfo-NHS-Biotinylation Kit according to the manufacturer's protocol (Thermo Fisher Scientific, San Jose, CA, USA). Biotin labelled GELNs were incubated with *P. gingivalis* for 1 h at room temperature with rotation. Biotin was pulled down by streptavidin magnetic beads (Thermo Fisher Scientific) and the beads were washed thoroughly with PBS to remove unbound protein. The protein bound magnetic beads were suspended in lysis buffer (2% SDS, 100 mM DTT, 20 mM Tris-HCl pH 8.8) at 95°C for 20 min. Protein was collected from supernatants after centrifugation and the concentration estimated using a Protein Assay Kit (Bio-Rad, Hercules, CA, USA). Protein aliquots (50 mg) were diluted into 4% SDS / 0.1M Tris-HCl

pH8.5 and 1M DTT and were processed according to the filter-aided sample preparation (FASP) method as described (Teng et al., 2017). The digested, ultra-filtered samples were trap-cleaned with C18 PROTO™, 300Å Ultra MicroSpin columns, lyophilized by vacuum centrifugation, re-dissolved into 16 µl of 2% v/v acetonitrile, and concentrations estimated based on absorption at 205 nm using a Nanodrop 2000 (Thermo Fisher Scientific).

**Liquid chromatography–mass spectrometry (LC-MS) data analysis**

Proteome Discoverer v1.4.1.114 (Thermo Fisher Scientific,) was used to analyze the data collected by the mass spectrometer. The database used in Mascot v2.5.1 and SequestHT searches was the 2/17/2017 version of the *P. gingivalis* proteome from UniprotKB (Proteome ID UP000236566). Scaffold was used to calculate the false discovery rate using the Peptide and Protein Prophet algorithms. Proteins were grouped to satisfy the parsimony principle. The proteins were clustered based on differential expression and heat maps representing differentially regulated proteins by GELNs were generated using software R.

**Monotypic biofilm assay.**

*P. gingivalis* biofilm was quantified using a microtiter plate assay. Saliva was collected in a sterile centrifuge tube on ice from healthy donors. DTT was added to a 2.5 mM final concentration, then centrifuged at 5,000 g for 10 min at $4^0$C. The clarified saliva supernatant was transferred, and 3 volumes of sterile distilled water added, and the 25% saliva was filtered through a 0.22 µm pore size filter. 96-well polystyrene cultured plate (Corning Inc., Corning, NY) was pre-coated with 25% saliva and incubated at $37^0$C for overnight. *P. gingivalis* strains were grown to mid-log phase ($OD_{600}$ = 0.8) and aliquots (200 µl) of samples were anaerobically incubated in the 25% saliva-coated wells with and without ginger exosomes like nano particles ($4.0 \times 10^8$ particles/ml) for 24 h. A sample (100 µl) of each cell culture was measured by optical density at 600 nm to assess planktonic bacterial growth. After discarding the planktonic bacterial cells in the wells, bacterial cells bound to the wells were gently washed three times with PBS, air dried, and then stained with 200 µl of 1% (w/v) crystal violet for 15 min. After washing twice with PBS and then with sterile

water to remove excess dye, the cell-bound dye was eluted using 200 μl of 95% ethanol. The absorbance was measured at 540 nm using 96-well plate reader (Molecular device).

**Animal infection**

Animal infection with *P. gingivalis* was carried out as described previously (Kuboniwa et al., 2017). Female 10-12-week-old C57BL/6 mice were obtained from Jackson Laboratories, maintained in groups and housed in micro isolator cages. Mice were a fed standard diet with water *ad libitum* and kept on a 12 h light and dark cycle. Animal care was performed following the Institute for Laboratory Animal Research (ILAR) guidelines and all animal experiments were done in accordance with protocols approved by the University of Louisville Institutional Animal Care and Use Committee (Louisville, KY). Before oral inoculation, mice were initially treated with sulfamethoxazole (800 μg/ml) and trimethoprim (400 μg/ml) ad libitum in water for ten days at two-day intervals. The mice were divided into four groups (five animals per group): control (uninfected) provided regular water, *P. gingivalis* infected provided regular water, *P. gingivalis* infected and provided GELNs containing water, control (uninfected) provided GELNs in water. *P. gingivalis* was suspended in 1 ml of 2% carboxymethylcellulose (CMC) and orally inoculated into mice at two-day intervals over a ten-day period. Mice were given GELN ($4.0 \times 10^8$ particles /ml) *ad libitum* in drinking water. To enumerate the colonization of *P. gingivalis*, oral samples were collected along the gingiva of the upper molars using a sterile polyester-tipped applicator at one, two and three weeks after the final bacterial infection. Total genomic DNA was isolated from these samples using a QIAamp DNA isolation kit (Qiagen) and amplified by qPCR with primers to 16s rRNA Forward 5'-AGGAACTCCGATTGCGAAGG-3' and reverse 5'-TCGTTTACTGCGTGGACTACC-3. Numbers of *P. gingivalis* were calculated using a standard curve derived from known amounts of *P. gingivalis*. Forty-two days after the last infection, mice were euthanized and skulls were subjected to μCT scan (SKYSCAN 1174, Bruker). Bone loss was assessed by measuring the distance between the alveolar bone crest and the cementoenamel junction at 14 predetermined points on the maxillary molars. For bone volume analysis, a region of interest (ROI) was drawn manually on the axial planes, between the medial root surface of the first molar and distal root

surface of the third molar. A three-dimensional image was generated from the ROI. All root volumes were excluded from the ROI to calculate the total volume (TV). The bone volume fraction (BV/TV) was calculated for each sample.

**Histology and immunofluorescence staining**

Oral tissue specimens were decalcified with 0.5 M EDTA (pH 7.4) for 3-4 weeks and processed for paraffin embedding. Tissue samples were cut at 5 μm thickness and stained with hematoxylin. For immunofluorescence analysis, tissue sections were subjected to antigen retrieval by boiling the slides in antigen unmasking solution (Vector laboratories) for 10 min according to the manufacturer's instructions. Sections were blocked with 5% BSA in PBS for 1 h at room temperature and incubated with the primary antibodies (1: 100) anti-rabbit-CD3, anti-CD45 or F4/80 at 4°C overnight. After extensive washing with PBS, tissue sections were incubated with Alexa 568-conjugated IgG and Alexa 488-conjugated IgG (1: 5000 dilution) for 1 h at room temperature. Nuclear staining was performed with DAPI for 15 min and images were captured by confocal microscopy (Nikon). To determine the number of osteoblasts, the sections were incubated with anti-rabbit-RUNX2 antibody (1:100) overnight at 4°C. HRP-conjugated anti-rabbit (1:5000) was used as secondary antibody and DAB chromogen was used as substrate. The slides were counterstained with hematoxylin. Similarly, the number of osteoclasts was determined using sections stained with TRAP (Sigma) according to manufacturer's protocol. The slides were counterstained with hematoxylin. The number of osteoblasts and multinucleated osteoclasts was counted manually.

**Statistical analysis**

Values are shown as mean ± SD for three independent experiments. Statistical analysis was performed with GraphPad Prism 6. Comparison of multiple experimental groups was performed using the one-way Analysis of Variance test. A $t$-test was used to compare the means of two groups. $P$ values of $< 0.05$ were considered to be statistically significant. Appropriate sample sizes were calculated to ensure statistical significance could be determined.

**SUPPLEMENTAL REFERENCES:**

Baginski, E.S., Epstein, E., and Zak, B. (1972). The measurement of serum total phospholipids. Annals of clinical laboratory science *2*, 255-267.

Bender, R.A. (2012). Regulation of the histidine utilization (hut) system in bacteria. Microbiology and molecular biology reviews : MMBR *76*, 565-584.

Christgen, S.L., and Becker, D.F. (2018). Role of Proline in Pathogen and Host Interactions. Antioxidants & redox signaling.

Conner, R.M., and Hansen, P.A. (1967). Effects of valine, leucine, and isoleucine on the growth of Bacillus thuringiensis and related bacteria. Journal of invertebrate pathology *9*, 12-18.

Cozzone, A.J. (2005). Role of protein phosphorylation on serine/threonine and tyrosine in the virulence of bacterial pathogens. Journal of molecular microbiology and biotechnology *9*, 198-213.

Cusumano, Z.T., and Caparon, M.G. (2015). Citrulline protects Streptococcus pyogenes from acid stress using the arginine deiminase pathway and the F1Fo-ATPase. Journal of bacteriology *197*, 1288-1296.

Delavier-Klutchko, C., and Flavin, M. (1965). Role of a Bacterial Cystathionine-Beta-Cleavage Enzyme in Disulfide Decomposition. Biochimica et biophysica acta *99*, 375-377.

Deng, X., Chen, K., Luo, G.Z., Weng, X., Ji, Q., Zhou, T., and He, C. (2015). Widespread occurrence of N6-methyladenosine in bacterial mRNA. Nucleic acids research *43*, 6557-6567.

El Qaidi, S., Yang, J., Zhang, J.R., Metzger, D.W., and Bai, G. (2013). The vitamin B(6) biosynthesis pathway in Streptococcus pneumoniae is controlled by pyridoxal 5'-phosphate and the transcription factor PdxR and has an impact on ear infection. Journal of bacteriology *195*, 2187-2196.

Ferla, M.P., and Patrick, W.M. (2014). Bacterial methionine biosynthesis. Microbiology *160*, 1571-1584.

Fuchs, G., Boll, M., and Heider, J. (2011). Microbial degradation of aromatic compounds - from one strategy to four. Nature reviews Microbiology *9*, 803-816.

Gillner, D.M., Becker, D.P., and Holz, R.C. (2013). Lysine biosynthesis in bacteria: a metallodesuccinylase as a potential antimicrobial target. Journal of biological inorganic chemistry : JBIC : a publication of the Society of Biological Inorganic Chemistry *18*, 155-163.

Hammes, W., Schleifer, K.H., and Kandler, O. (1973). Mode of action of glycine on the biosynthesis of peptidoglycan. Journal of bacteriology *116*, 1029-1053.

Hart, G.W. (1982). The role of asparagine-linked oligosaccharides in cellular recognition by thymic lymphocytes. Effects of tunicamycin on the mixed lymphocyte reaction. The Journal of biological chemistry *257*, 151-158.

Kolodkin-Gal, I., Romero, D., Cao, S., Clardy, J., Kolter, R., and Losick, R. (2010). D-amino acids trigger biofilm disassembly. Science *328*, 627-629.

Kuboniwa, M., Houser, J.R., Hendrickson, E.L., Wang, Q., Alghamdi, S.A., Sakanaka, A., Miller, D.P., Hutcherson, J.A., Wang, T., Beck, D.A.C.*, et al.* (2017). Metabolic crosstalk regulates Porphyromonas gingivalis colonization and virulence during oral polymicrobial infection. Nature microbiology *2*, 1493-1499.

Kutanovas, S., Stankeviciute, J., Urbelis, G., Tauraite, D., Rutkiene, R., and Meskys, R. (2013). Identification and characterization of a tetramethylpyrazine catabolic pathway in Rhodococcus jostii TMP1. Applied and environmental microbiology *79*, 3649-3657.

Liu, P., Zhang, H., Lv, M., Hu, M., Li, Z., Gao, C., Xu, P., and Ma, C. (2014). Enzymatic production of 5-aminovalerate from L-lysine using L-lysine monooxygenase and 5-aminovaleramide amidohydrolase. Scientific reports *4*, 5657.

Luo, S., and Levine, R.L. (2009). Methionine in proteins defends against oxidative stress. FASEB journal : official publication of the Federation of American Societies for Experimental Biology *23*, 464-472.

Meadows, J.A., and Wargo, M.J. (2015). Carnitine in bacterial physiology and metabolism. Microbiology *161*, 1161-1174.

Melander, R.J., Minvielle, M.J., and Melander, C. (2014). Controlling bacterial behavior with indole-containing natural products and derivatives. Tetrahedron *70*, 6363-6372.

Moura, A.P., Ribeiro, C.A., Zanatta, A., Busanello, E.N., Tonin, A.M., and Wajner, M. (2012). 3-Methylcrotonylglycine disrupts mitochondrial energy homeostasis and inhibits synaptic Na(+),K (+)-ATPase activity in brain of young rats. Cellular and molecular neurobiology *32*, 297-307.

Muto, A., and Osawa, S. (1987). The guanine and cytosine content of genomic DNA and bacterial evolution. Proceedings of the National Academy of Sciences of the United States of America *84*, 166-169.

Rao, D.R., and Rodwell, V.W. (1962). Metabolism of pipecolic acid in a Pseudomonas species. I. alpha-Aminoadipic and glutamic acids. The Journal of biological chemistry *237*, 2232-2238.

Simionato, M.R., Tucker, C.M., Kuboniwa, M., Lamont, G., Demuth, D.R., Tribble, G.D., and Lamont, R.J. (2006). Porphyromonas gingivalis genes involved in community development with Streptococcus gordonii. Infection and immunity *74*, 6419-6428.

Teng, Y., Ren, Y., Hu, X., Mu, J., Samykutty, A., Zhuang, X., Deng, Z., Kumar, A., Zhang, L., Merchant, M.L.*, et al.* (2017). MVP-mediated exosomal sorting of miR-193a promotes colon cancer progression. Nature communications *8*, 14448.

Viala, J.P., Meresse, S., Pocachard, B., Guilhon, A.A., Aussel, L., and Barras, F. (2011). Sensing and adaptation to low pH mediated by inducible amino acid decarboxylases in Salmonella. PloS one *6*, e22397.

Wargo, M.J. (2013). Homeostasis and catabolism of choline and glycine betaine: lessons from Pseudomonas aeruginosa. Applied and environmental microbiology *79*, 2112-2120.

Xiong, L., Teng, J.L., Botelho, M.G., Lo, R.C., Lau, S.K., and Woo, P.C. (2016). Arginine Metabolism in Bacterial Pathogenesis and Cancer Therapy. International journal of molecular sciences *17*, 363.